Theses and Dissertations

Theses, Dissertations, and Senior Projects

January 2016

Comparison And Evaluation Of Precipitation Products From Radar, Satellite, And Reanalyses Over The Continental United States

Wenjun Cui

Follow this and additional works at: https://commons.und.edu/theses

COMPARISON AND EVALUATION OF PRECIPITATION PRODUCTS FROM RADAR, SATELLITE, AND REANALYSES OVER THE CONTINENTAL UNITED STATES

by

Wenjun Cui
Bachelor of Science, Nanjing University of Information Science and Technology, 2014

A Thesis
Submitted to the Graduate Faculty

of the

University of North Dakota

In partial fulfillment of the requirements

for the degree of

Master of Science

Grand Forks, North Dakota
August
2016

This thesis, submitted by Wenjun Cui in partial fulfillment of the requirements for the Degree of Master of Science from the University of North Dakota, has been read by the Faculty Advisory Committee under whom the work has been done, and is hereby approved.

<div style="text-align: right">

_____
Xiquan Dong

_____
Baike Xi

_____
Aaron Kennedy

</div>

This thesis is being submitted by the appointed advisory committee as having met all of the requirements of the Graduate School at the University of North Dakota and is hereby approved.

_____
Dr. Grant McGimpsey
Dean of the Graduate School

_____
Date

PERMISSION

Title   Comparison and Evaluation of Precipitation Products from Radar, Satellite,
                 and Reanalyses over the Continental United States

Department   Atmospheric Sciences

Degree   Master of Science

In presenting this thesis in partial fulfillment of the requirements for a graduate degree from the University of North Dakota, I agree that the library of this University shall make it freely available for inspection. I further agree that permission for extensive copying for scholarly purposes may be granted by the professor who supervised my thesis work or, in their absence, by the chairperson of the department or the dean of the School of Graduate Studies. It is understood that any copying or publication or other use of this dissertation or part thereof for financial gain shall not be allowed without my written permission.   It is also understood that due recognition shall be given to me and to the University of North Dakota in any scholarly use which may be made of any material in my thesis.

Signature: Wenjun Cui

Date: 07/21/2016

TABLE OF CONTENTS

vi

LIST OF FIGURES

ix

LIST OF TABLES

ACKNOWLEDGEMENTS

ABSTRACT

To better understand the precipitation variability over the continental United States (CONUS), an accurate temporally and spatially homogenous precipitation dataset should be used. Recently developed precipitation products, including satellite-based, radar-based, and atmospheric reanalysis products appear to fit these criteria, however, their uncertainties must first be addressed. This study is divided into two parts. Part I focuses on a comparison between satellite-based GPCP IDD estimates and radar-based NMQ Q2 estimates, offering physical insight into the differences between the two datasets. Part II evaluates the precipitation estimates from five reanalysis products, and studies the precipitation trend over the CONUS over the last three decades using GPCP monthly product, where the uncertainties associated with GPCP datasets found in part I will be addressed.

In part I of this study, spatial averages of monthly and yearly accumulated precipitation were computed based on daily estimates from the six selected regions during the period from 2010 through 2012. Correlation coefficients for daily estimates over the selected regions range from 0.355 to 0.516 with mean differences (GPCP-Q2) varying from -0.86 to 0.99 mm. Better agreements are found in monthly estimates with the correlations varying from 0.635 to 0.787. The comparisons between two datasets are also conducted for warm (April-September) and cold (October-March) seasons. During the warm season, GPCP estimates are 9.7% less than Q2 estimates, while during the cold season GPCP estimates exceed Q2 estimates by 6.9%. For precipitation over the CONUS,

although annual means are close (978.54 mm for Q2 vs. 941.79 mm for GPCP), Q2 estimates are much higher than GPCP over the central and southern CONUS and lower than GPCP estimates in the northeastern US. These results suggest that Q2 may have difficulty accurately estimating heavy rain and snow events, while GPCP may have an inability to capture some intense precipitation events, which warrants further investigation.

In part II of this study, precipitation estimates from five reanalyses (ERA-Interim, MERRA2, JRA-55, CFSR, and 20CR) are compared against the GPCP satellite-gauge (SG) combined product over the CONUS during the period from 1980 through 2013. Compared to the annual averaged precipitation of 2.38 mm/day from GPCP, CFSR has the same annual mean, ERA-Interim and MERRA2 have negative biases of -9.2% and -3.8% respectively, while JRA-55 and 20CR have positive biases of 9.7% and 12.6% respectively. The reanalyses capture the variability of precipitation distribution over the CONUS as derived from GPCP; however, large regional differences exist. The reanalyses generally overestimate the precipitation over the western part of the country throughout the year, which could be due to the difficulty of accurately estimating precipitation over complex terrain. Underestimations in reanalyses over the northeastern US during fall and winter seasons indicate that the five selected reanalyses may be less skillful in reproducing snowfall events. Furthermore, systematic errors exist in all five reanalysese suggest that their physical processes in modeling precipitation need to be improved in the future. We also conduct a long-term trend analysis of precipitation over the CONUS

using GPCP and reanalyzed precipitation products from 1980 to 2013. Based on the linear regression of GPCP data, there is a decreasing trend of 2.00 mm/year. For spatial distribution, only north-central and northeastern parts of the county show positive trends, while other areas show negative trends on through the course of a year. Compared to the GPCP observed long-term trend of precipitation, all reanalyses except for 20CR exhibit similar inter-annual variation. Although comprehensive reanalyses that assimilate both satellite and in-situ observations can provide more reasonable precipitation estimates, substantial efforts are still required to further improve the reanalyzed precipitation over the CONUS.

CHAPTER I

INTRODUCTION

Background

Precipitation is a critical component of land surface processes and the hydrological cycle. It is also an important factor for understanding climate variability. Changing rainfall patterns have a significant impact on water sources, and directly influence industrial and agricultural output as well as people's daily lives. The characteristics of precipitation over the continental United States (CONUS) differ significantly in time and space, which is the result of the interaction of several complex atmospheric and oceanic processes evolving at different spatial and temporal scales. During the Northern Hemisphere summer, a subtropical ridge in the Atlantic Ocean often transports warm and humid air from the Atlantic Ocean and the Gulf of Mexico over the continent (Benton and Estoque 1954), aiding development of thunderstorms over the southern tier of the country as well as Great Plains. Obtaining the moisture from air masses that flow from Pacific Ocean, the western CONUS receives most of its precipitation during the winter (Holzman 1937). Nor'easters moving up the East coast bring cold season precipitation to the northeastern United States (Davis and Dolan 1993). Meanwhile, lake-effect snow adds precipitation to the Great Lakes regions during the cold season (Burnett et al. 2003). Sensitive to the variations in rainfall distribution, the changes in precipitation pattern in the CONUS will lead to the increase or decrease in precipitation amounts, and hence it

may lead to large-scale precipitation extremes (e.g. droughts and floods).

Precipitation can be directly observed from ground-based measurements (e.g. rain gauges), which provide relative accurate rainfall estimates at point locations. However, in regions with sparse rain gauge coverage such as oceans and unpopulated areas, rain gauge measurements may not capture the spatial and temporal variability of precipitation events (Villarini et al. 2008). Radar provides high spatial and temporal resolution rainfall estimates, but several sources of uncertainty are associated with radar-based estimates including attenuation, ground clutter, beam blockage, beam height, and variability in the *Z-R* relationships (Wilson and Brandes 1979). Additionally, sufficient radar coverage for radar-based estimates is not widespread outside of the United States, Europe, and Japan. For complete global precipitation information, satellite-based and atmospheric reanalysis datasets are relied upon; however, these often suffer from relatively large uncertainties (Xie and Arkin, 1997; Huffman et al. 2001; Tian and Peters-Lidard. 2010).

Satellite-based precipitation retrievals are typically calculated either from empirical relationships between measured cloud-top temperature from infrared (IR) instruments and precipitation rates, or passive microwave (PMW) instrument data which directly measure the scattering of upwelling radiation as well as the thermal emission from raindrops and hydrometers to estimate precipitation rate (Joyce et al. 2004). IR sensors onboard geostationary satellites can provide precipitation estimates at high temporal resolution, but errors may occur where rainfall does not correlate well with cloud-top temperature (i.e., nonprecipitating cirrus clouds, tropical warm clouds). Microwave

sensors measure precipitation in a more direct way but are only aboard polar-orbiters, and therefore have a significant limitation in spatial and temporal sampling (Joyce et al. 2004). With the limitations intrinsic in the independent measurements in mind, new techniques have been developed to combine IR and PMW sensors on multiple satellites in order to produce global precipitation estimates by making use of the advantages of each sensor. Since the lunch of Tropical Rainfall Measuring Mission (TRMM) in late 1997, precipitation techniques and algorithms have been devised and modified to combine IR and microwave observations to provide real-time precipitation information. To date, numerous satellite precipitation products have been released with various temporal and spatial resolutions, including Precipitation Estimation from Remotely Sensed Information Using Artificial Neural Networks (PERSIANN; Sorooshian et al. 2000); Climate Prediction Center morphing technique (CMORPH; Joyce et al. 2004); TRMM Multi-satellite Precipitation Analysis (TMPA; Huffman et al. 2007, 2010); Global Precipitation Mission Integrated Multi-satellite Retrievals (GPM IMERG; Huffman et al. 2014); and Global Precipitation Climatology Project 1 Degree Daily (GPCP 1DD; Huffman et al. 2001), which will be used in this study.

GPCP 1DD is based on the combination of data from multiple satellites and provides global daily precipitation estimates on a one degree grid box from 1996 to present. Recent adjustments and improvements have helped GPCP 1DD provide more reasonable precipitation estimates, such as the transition from Television Infrared Operational Satellite (TIROS) Operational Vertical Sounder (TOVS) data to Advanced Infrared

Sounder (AIRS) data for precipitation estimates poleward of 40° latitude in April 2005 and the release of Version 1.2 of GPCP 1DD precipitation dataset in September 2012 (Huffman and Bolvin 2013). Nonetheless, the satellite-based techniques are associated with errors resulting from sampling data from different instruments and satellites, inaccurate estimates from precipitation algorithms under certain conditions, and the instruments themselves. Therefore, the accuracy of GPCP 1DD estimates should be determined through careful comparisons with alternative high spatial and temporal resolution and coverage datasets.

In addition to combining data from different satellites, global precipitation datasets can also be generated by merging rain gauge observations with satellite analysis. One such product is GPCP satellite-gauge (SG) combined product. GPCP SG produces monthly precipitation estimates by combing precipitation information available from each source into a final merged product, taking advantage of the strengths of each data type and removing biases based on hierarchical relations in the stepwise approach (Adler et al. 2003). Updated to version 2.2 in 2012, the GPCP SG dataset takes advantage of upgrades in many of the constituent datasets, including the Chang/Chiu/Wilheit (CCW) emission and National Oceanic and Atmospheric Administration (NOAA) scattering algorithms, the updated Global Precipitation Climatology Centre (GPCC) precipitation gauge analysis, as well as the inclusion of the Defense Meteorological Satellite Program (DMSP) F18 SSIMS (Huffman and Bolvin, 2013). With advanced precipitation estimation techniques, GPCP SG has been used as reference data for many trend analyses

and validation studies (Gu et al. 2007; Fensholt et al. 2011; Stanfield et al. 2015; Hatzianastaasiou et al. 2016). To reduce the inconsistency between GPCP products with different temporal scales, the monthly SG precipitation estimates are used to calibrate the 1DD daily estimates, and the monthly sums of 1DD estimates are computed to match the monthly SG precipitation estimates. With relatively adequate satellite and GPCC gauge sampling over the CONUS, the estimates from GPCP SG might be a suitable tool to investigate the long-term pattern of precipitation over the US.

Atmospheric reanalysis datasets have been widely used in climate research because of their spatial and temporal continuity. Reanalyses are generated through a consistent data assimilation system and model, which incorporates all available observations and a background model forecast to generate uniform gridded data (Bosilovich et al. 2008). With continuous improvements in data assimilation methods and numerical models, and the increasing availability of observation data from satellite and in-situ measurements, recently developed reanalysis datasets can produce reasonable output of atmospheric and oceanic variables for climate studies. However, errors and uncertainties can still be raised from aspects such as poor data quality, deficiency in model physical parameterizations, and inhomogeneities introduced by changes in observing system.

Global reanalysis datasets do not directly generate precipitation analysis. In other words, precipitation is not a control variable in the analysis procedure (Rienecker et al. 2011), and thus the precipitation in reanalysis is highly related to the physical parameterization in modeling system. For instance, Rienecker et al. (2011) concluded that

even though microwave-retrieved rain rate observations are assimilated into model over oceans, humidity information derived from passive microwave measurements was found to have a much larger impact on the precipitation than precipitation observation themselves in the Modern-Era Retrospective analysis for Research and Applications (MERRA) reanalysis. Therefore, errors may occur when models cannot simulate the physical mechanisms responsible for precipitation. In addition, the precipitation estimates in reanalysis products are also influenced by the changes in observational data, including the coverage and continuity of observation stations, radiosondes and satellite instruments, and this can leads to abrupt changes in precipitation records. Hence, the discontinuities introduced by changing observing systems may be found in reanalyzed climate data. To better understand and quantify the uncertainties in the precipitation estimates generated by reanalyses, comparisons with observation-based precipitation datasets should be performed.

<div align="center">Previous Studies</div>

To date, several studies have been conducted to examine the performance of GPCP 1DD and reanalysis precipitation estimates (Huffman et al. 2001; Mcphee and Margulis 2005; Gebermichael et al. 2005; Bolvin et al. 2009; Joshi et al. 2012; Ma et al. 2009; Wang and Zeng 2012; Bosilovich 2013; Lee and Biasutti 2014; Blacutt et al. 2015; Dolinar et al. 2015; Prakash et al. 2015). Rana et al. (2015) evaluated GPCP 1DD, rain gauge, and reanalysis data against the Asian Precipitation-Highly-Resolved Observational Data Integration Towards Evaluation of the Water Resources (APHRODITE). They found

that GPCP 1DD estimates performed better than reanalysis data and were well correlated with APHRODITE. Alemohammad et al. (2015) investigated the uncertainties in NEXRAD-IV, TRMM 3B42RT, GPCP 1DD and the Geostationary Operational Environmental Satellite (GOES) Precipitation Index (GPI) precipitation products using triple collocation (TC) technique over the central part of the COUNS. The results indicated that GPCP 1DD, NEXRAD, and TRMM 3B42RT products had similar climatological pattern across the domain while GPI was different. However, GPCP 1DD and GPI products had poorer quality of precipitation estimates than NEXRAD and TRMM 3B42RT.

With regard to reanalyzed precipitation, Bosilovich et al. (2008) evaluated global precipitation from five reanalyses using GPCP and the Climate Prediction Center (CPC) merged Analysis of Precipitation (CMAP) during the period 1979-2005. Results showed that ERA-40 produced reasonable precipitation estimates over Northern Hemisphere continents, but less so over the tropical oceans. Japanese 25-year Reanalysis (JRA-25) performed better than ERA-40 over both Northern Hemisphere continents and tropical oceans but contained distinct variations in time depending on the available observing systems. Kishore et al. (2015) validated four reanalysis datasets with gridded India Meteorological Department (IMD) rainfall datasets over the Indian subcontinent, and concluded that all reanalyses captured the strong inter-annual variations within the Indian region well, and of all reanalysesERA-Interim showed more realistic values with respect to IMD observations. Pfeifroth et al. (2013) examined the ERA-Interim and MERRA

over the tropical pacific regions using gauge station data provided by Pacific Rainfall Database (PACRAIN) and found that both reanalysis products show similar systematic behaviors in overestimating light and medium precipitation events and underestimating heavier events. Ashouri et al. (2016) evaluated the skill of MERRA in reproducing historical extreme precipitation events in the United States with gauge-based CPC Unified data and showed that MERRA reasonably mimics the continental-scale patterns of change as observed by CPC while underestimating magnitude of extremes, particularly over the Gulf Coast regions.

Purpose

In the first part of this study, GPCP 1DD precipitation product is compared with the National Mosaic and Multi-Sensor Next Generation Quantitative Precipitation Estimation System (NMQ Q2) over the central and eastern parts of Continental United States (CONUS) during the period 2010-12. NMQ Q2 composites radar data from the Weather Surveillance Radar-1988 Doppler (WSR-88D) network, producing instantaneous precipitation estimates at a high spatial and temporal resolution. Recent evaluation studies of the Q2 product suggest that Q2 estimates are viable as a validation tool for satellite precipitation retrievals in lieu of ground-based measurements in the future (Chen et al. 2014; Stenz et al. 2014). Uncertainties, however, still exist in radar-derived precipitation estimates as mentioned in the beginning of this section. Because evaluations of Q2 estimates over large domains have only been performed against surface rain-gauge measurements (Wu et al. 2012; Chen et al. 2014), the comparison between radar-based

Q2 estimate and satellite-based GPCP 1DD estimate not only directly shows the difference between the active and passive sensing data, but may also provide insight into the existing and potential limitations and strengths of each dataset. Different time scales, from daily to annual, are used to investigate possible errors that may associated with Q2 and GPCP 1DD estimates changing with different time scales. Because the GPCP 1DD monthly accumulated precipitation estimates match the GPCP SG estimates, the comparison may also reveal the uncertainties within the SG product. It should be noted that this is not a validation study, and neither GPCP 1DD nor Q2 estimates are treated as ground truth to validate the other.

The second part of this study evaluates the long-term performance of precipitation data from five reanalysis products, including ERA-Interim, MERRA Version-2 (MERRA2), Japanese 55-year Reanalysis (JRA-55), Climate Forecast System Reanalysis (CFSR), and NOAA-CIRES 20th Century Reanalysis Version 2c (20CRv2c) using the GPCP SG product over the CONUS during the period from 1980 through 2013. Since the precipitation in reanalyses are not only closely related to model parameterizations, but also related to the assimilated data, the evaluation against GPCP will provide an insight into how model and the observing system influence the precipitation output. Furthermore, although the assimilated input data in the reanalysis datasets are similar, an intercomparison between reanalyses will provide a better understanding of their differences in assimilation systems, physical parameterizations, and processing methodologies of input data. During the evaluation, the uncertainties of GPCP SG

product concluded from part I of this study will be addressed. A trend analysis is also conducted based on the GPCP SG product from 1980 through 2013 to investigate the seasonal and annual precipitation tendencies, as well as the regional trends over the CONUS.

The outline of this thesis is as follows: Chapters II and III describe the data and methods used in this study. Chapter IV shows results of a comparison between GPCP 1DD and Q2 daily estimates and intercomparions of reanalysis products use GPCP SG as a reference. Chapter V discusses the findings from Chapter IV. Finally, the summary is provided in Chapter VI.

CHAPTER II

DATA

Global Precipitation Climatology Project (GPCP) Daily and Monthly Products

The GPCP product is developed at the National Aeronautics and Space Administration (NASA) Goddard Space Flight Centre as a part of the Global Energy and Water Exchanges Project (GEWEX; Arkin and Xie 1993). In this study, both the daily and monthly products are used. The GPCP 1DD daily estimates are compared with Q2 estimates in part I of this study. In part II, the GPCP SG monthly accumulated precipitation estimates are used as a validation tool for the reanalysis datasets and for trend analysis.

GPCP Satellite-Gauge (SG) Combined Monthly Product (Version 2.2)

The GPCP SG combined product provides global monthly precipitation estimates on a 2.5° (latitude) × 2.5° (longitude) grid from combined multi-satellite and gauge observations, and is available from January 1979 to present (Adler et al. 2003). The monthly dataset contains 27 precipitation products. For the pre-Special Sensor Microwave Imager-Sounder (SSMIS) period (1979-1986), the GPCP satellite component is based on the outgoing longwave radiative (OLR) Precipitation Index (OPI) technique that retrieves precipitation using Infrared (IR) observations from low-Earth orbit satellites (Xie and Arkin 1998). After multiple meteorological satellites were launched in 1986, more satellite-based retrieval algorithms were developed and introduced to improve the GPCP dataset. Additions included SSMI (SSMIS) estimates calculated from the Wilheit

et al. (1991) emission and Grody (1991) scattering algorithms that retrieve precipitation

from the quantity of liquid water/ice hydrometeor in a column from observed brightness

temperatures; TOVS and AIRS estimates based on the methods of Susskind and

Pfaendtner (1989) and Susskind et al. (1997) that infer precipitation from deep, extensive

clouds; GPI (Arkin and Meisner 1987) product that estimates precipitation based on the

empirical relationship between rain rate and IR brightness temperature. The GPI values

are merged with SSMI (SSMIS) estimates calibrated by TOVS (AIRS) data between

40°S to 40°N, while for Polarward of 40°, they are merged with SSMI (SSMIS)/TOVS

(AIRS) data. The preliminary satellite fields from both pre-SSMI and SSMI periods are

climatologically calibrated with the gauge data from GPCC over the large-scale domain.

Then the gauge-adjusted satellite precipitation estimates are merged with GPCC gauge

analyses for each grid box using the inverse variance weighting method to form the final

SG monthly product. A more detailed description of input datasets and merging methods

used in GPCP product can be found in Alder et al. (2003), Huffman et al. (2009), and

Huffman and Bolvin, (2012).

GPCP One Degree Daily (1DD) product (Version 1.2)

GPCP 1DD Version 1.2 provides global daily precipitation estimates on a 1° × 1°

grid from combined satellite observations. Between 40°S and 40°N, rainfall estimates are

computed using the Threshold-Matched Precipitation Index (TMPI), which utilizes

fractional occurrence of precipitation calculated by the Goddard Profiling Algorithm

(GPROF; Kummerow et al. 1996) Version 2004 using SSMI-SSMIS data, the

12

geostationary IR (geo-IR) brightness temperature histograms from the Geostationary Satellite Precipitation Data Centre (GSPDC), and precipitation rates computed by the GPI based on low-earth orbit IR (leo-IR) data. The TMPI provides GPI-like precipitation estimates, but unlike the GPI, which assigns a conditional rain rate to all pixels within a given region that have a brightness temperature (T_b) below a brightness temperature threshold (T_{b0}), TMPI allows both T_{b0} and conditional rain rate to vary with space and time (Huffman et al. 2001). For each grid box, T_{b0} is obtained by accumulating the geo-IR histograms until the fraction of pixels matches the occurrence of precipitation. The conditional rain rate is then calculated by dividing GPCP satellite-gauge (SG) monthly estimates by the frequency of pixels below the T_{b0}. The rain rate estimates from leo-IR GPI are processed to fill in gaps where there is no geo-IR data. Poleward of 40°S and 40°N, the precipitation estimates through March of 2005 are computed from TOVS data. Since April of 2005, AIRS data have been used in place of TOVS data. The TOVS-AIRS technique estimates precipitation using a multiple regression relationship between collocated rain gauge measurements and various atmospheric parameters including cloud-top pressure, fractional cloud cover, and relative humidity profiles (Susskind et al. 1997; Susskind and Pfaendtner 1989). Additionally, monthly sums of both TMPI and TOVS-AIRS daily estimates are computed and matched to the monthly SG precipitation estimates, which reduces the inconsistency between the products with different temporal scales.

NMQ Q2

NMQ Q2 combines information from all ground-based radars in the Next-Generation Radar (NEXRAD) network, and provides precipitation estimates with a horizontal resolution of 1km × 1km and a temporal resolution of 5 minutes over the CONUS (Chen et al. 2013). Reflectivity data from multiple radars are mosaicked onto a common 3 dimensional grid, then each vertical reflectivity column is objectively analyzed and prescribed a precipitation type (i.e., convective, stratiform, warm rain) if precipitation is present. The Z-R relationship determined by classified precipitation type will be assigned to each grid cell to estimate rainfall. Four Z-R relationships are used in association with the precipitation type in Q2 (Zhang et al. 2011): Convective (Fulton et al. 1998): $Z = 300R^{1.4}$; Stratiform (Marshall et al. 1955): $Z = 200R^{1.6}$; Warm rain (Rosenfield et al. 1993): $Z = 230R^{1.25}$; and snow at the surface (Zhang et al. 2011): $Z = 75R^{2.0}$.

Global Reanalysis Products

In part II of this study, the simulated precipitation from five global reanalysis datasets (ERA-Interim, MERRA2, JRA-55, CFSR, and 20CRv2c) are compared and evaluated with GPCP SG monthly product during the period from 1980 through 2013 over the CONUS. A general summary of each reanalysis dataset, including horizontal and spatial resolutions, temporal ranges, assimilation types and references, is shown in the Table 1.

Table 1. Summary of the reanalyses used in this study.

Reanalysis	Model resolution	Assimilation method	Horizontal grid spacing (lat×lon)	Temporal range	Reference
ERA-Interim	T255 L60	4D-VAR	0.75°×0.75°	01/1979-present	Dee et al. (2011)
MERRA2	72 sigma level	3D-VAR	0.625°×0.5°	01/1980-present	Rienecker et al. (2011) Bosilovich et al. (2015)
JRA-55	T319 L60	4D-VAR	1.25°×1.25°	01/1958-12/2013	Kobayashi et al. (2015)
CFSR	T382 L64	3D-VAR	0.5°×0.5°	01/1979-present	Saha et al. (2010)
20CR	T62 L28	Ensemble Kalman Filter	2°×2°	01/1958-12/2014	Compo et al. (2011)

European Centre for Medium-Range Weather Forecasts (ECMWF) ERA-Interim

ERA-Interim was developed by the ECMWF as a replacement for its preceding version - ERA-40, emphasizing several difficulties associated with data assimilation in the product of ERA-40, including the poor representation of hydrological cycle (Dee et al. 2011). The analyzed monthly precipitation estimates are produced based on a 12-hour segment forecast within the ERA-Interim model system. Assimilated SSM/I radiances data from geostationary satellites as well as data from radiosonde and ground-based measurements are used as important input to generate a humidity analysis field. Compared to ERA-40, the revised humidity analysis scheme and method for correcting biases in radiance data have helped ERA-Interim produce more reasonable precipitation

estimates with respect to observational-based precipitation product (Dee et al. 2011).

Modern-Era Retrospective analysis for Research and Applications version 2 (MERRA2)

MERRA2 is a NASA atmospheric reanalysis using a recent version of the Goddard Earth Observing System Model version 5 (GEOS-5) data assimilation system (DAS; Bosilovich et al. 2015). The changes in GEOS-5 include physical parameterizations for moist, surface, gravity wave drag module algorithms, and enables the MERRA2 to incorporate more observations from newer satellite instruments (Molod et al. 2015). MERRA2 uses an incremental analysis update that minimizes the spindown effects of the water vapor analysis. Although MERRA2 assimilates rain rate estimates from SSM/I and Tropical Rainfall Measuring Mission (TRMM) Microwave Imager (TMI) over the ocean, these data are given a low weight and have a weaker impact on the increments than the humidity information derived from satellite radiance data, as mentioned in the previous section. Over land, MERRA2 does not assimilate precipitation (Rienecker et al. 2011), therefore, it is similar to ERA-Interim in that it produces a water vapor analysis field using in-situ and satellite radiance data. The large-scale precipitation model is based on the scheme of Zhao and Carr (1997), which is sensitive to the moisture and cloud condensate over land (Rienecker et al. 2008).

The Japanese 55-Year Reanalysis (JRA-55)

The JRA-55 is the second Japanese global atmospheric reanalysis created by the Japan Meteorological Agency (JMA), available from 1958 when regular radiosonde

observations started becoming available globally. JRA-55 was first produced by the TL319 version of JMA's operational data assimilation system in December 2009. The newly available observations as well as the improved previous observations have helped JRA-55 produce considerably better analysis results than the JRA-25 (Kobayashi et al. 2015). To generate convection, a prognostic mass-flux type Arakawa-Schubert Scheme (Arakawa and Schubert 1974) with Downward Convective Available Potential Energy (DCAPE) is adopted for the cumulus parameterization in JRA-55. The vertical profile of upward mass flux is assumed to be linear with height (Moorthi and Suarez 1992) and the mass flux at the cloud base is determined by solving a prognostic equation (Randall and Pan 1993). The scheme was updated by Nakagawa and Shimpo (2004) by considering the effect of detrainment due to downdrafts instead of simply re-evaporating the precipitation which cools and moistens the lower troposphere, and this technique represents convective downdrafts more realistically (Onogi et al. 2007).

Climate Forecast System Reanalysis (CFSR)

CFSR is produced by the National Centers of Environmental Prediction (NCEP). It contains various upgrades in model physics and assimilation algorithms compared to the earlier NCEP/National Center for Atmospheric Research (NCAR) (R1, Kalnay et al. 1996) and NCEP/DOE (R2, Kanamitsu et al. 2002) reanalyses. Differing from other reanalysis datasets that use only an atmospheric model, CFSR coupled the new Global Forecast System (GFS) atmospheric model with Modular Ocean Model version 4 (MOM4) ocean model to assimilate and predict atmospheric states at every 6-hr. In each

17

analysis cycle, in situ and satellite observations are assimilated with the first guess obtained from 6-hr coupled forecast from the previous analysis to produce analyzed field. The new analysis is then taken as the background conditions for the next model forecast cycle (Saha et al. 2010). For the atmospheric forecast model, a simplified Arakawa-Schubert scheme (Arakawa and Schubert 1974; Pan and Wu 1995; Hong and Pan 1998) is used for the cumulus convection parameterization with cumulus momentum mixing and orographic gravity wave drag (Kim and Arakawa 1995; Alpert et al.). The shallow convection parameterization follows Tiedtke et al. (1983) for wherever the deep convection parameterization is not active.

Twentieth Century Reanalysis Version 2c (20CRv2c)

The 20CR project is an effort led by NOAA and the University of Colorado Cooperative Institute for Research in Environmental Sciences (CIRES) to produce a reanalysis dataset spanning the entire twentieth century, assimilating only the surface observations of sea level pressure (SLP), monthly sea surface temperature (SST) and sea ice distribution as boundary conditions. The 20CR version 2 uses the Ensemble Kalman Filter data assimilation approach (Whitaker and Hamill 2002),   yields each 6-hr analysis as the most likely state of the global atmosphere, and provides uncertainty estimates in the form of 56 realizations (Compo et al. 2011). 20CR uses the same model as the NCEP GFS 2008ex version 2. By applying a prognostic cloud condensate scheme, the precipitation rate is parameterized following the approaches of Zhao and Carr (1997) for ice and Sundqvist et al. (1989) for liquid water.

18

CHAPTER III

METHODOLGY

Part I: Comparison of GPCP 1DD with Q2 estimates

In part I of this study, the comparison between GPCP 1DD and Q2 estimates are conducted over six selected tiles/regions based on the NMQ domain shown in Fig. 1a. Tiles 1 and 5 as well as regions in tiles 2 and 6 west of 5º longitude have been excluded because of significant beam blockage over the mountainous regions (Fig. 1b). Tiles 2, 3 and 4 have northern and southern boundaries at 60°N and 40°N, while tiles 6, 7, and 8 are bounded by 40°N and 20ºN. Western and eastern boundaries range from 110ºW to 90ºW (105ºW to 90ºW in this study), including 90ºW – 80ºW for tiles 3 and 7, and 80ºW – 60ºW for tiles 4 and 8. The six selected tiles cover a total of 619 1º × 1º grid boxes.
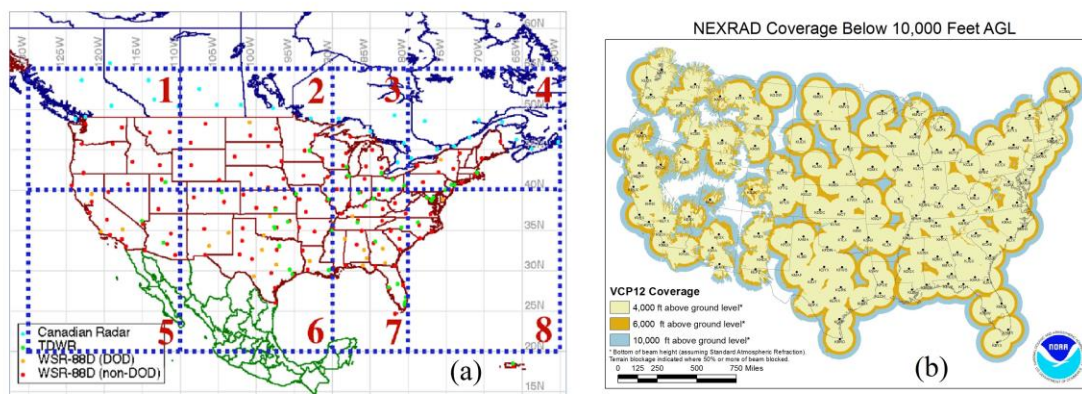
Figure 1. (a) NMQ product domain (dotted dark blue box) divided into eight tiles. Dots of different colors represent different radar networks: WSR-88D (yellow and red), Terminal Doppler Weather Radar (TDWR; green), and the operational Canadian weather radars (light blue). Image adapted from Grams (2013). (b) Map of NEXRAD radar locations and coverage over United States. Image provided by the NOAA/NWS/Radar Operational Center.

Q2 daily precipitation estimates from 2010 through 2012 are calculated by summing the hourly Q2 accumulated precipitation estimates each day. The 1km × 1km Q2 data are regridded into a 1º × 1º grid box by averaging the points within each grid in order to match the spatial resolution of GPCP 1DD. Next, concurring Q2 and GPCP 1DD grid boxes with zero accumulated precipitation are excluded. Furthermore, in order to investigate how the differences between the two datasets behave in different time-scales, monthly and annual accumulated precipitation are calculated by simply summing the daily estimates. For spatially averaged precipitation, the latitudinally weighted precipitation amounts are calculated for each grid box based on the latitude of that grid box. Then spatially averaged precipitation amounts are computed for daily and monthly estimates by adding up weighted precipitation values of grid boxes within the tile and divided by the total number of grid boxes. Scatterplots are made between the Q2 and GPCP 1DD for daily, monthly, and annual estimates, as well as spatial averages along with their corresponding linear regression fits for the six selected regions. The short- and long-term estimates of these two datasets and their differences can be examined and compared by different time scale analyses. Note that the Q2 daily estimates over some regions suffer from poor radar coverage which impacts estimated precipitation, however, the problem is not as severe as over tiles 1 and 5. Therefore, these daily estimates are used in the comparisons, and their uncertainties or errors are discussed in this study.

The comparisons over the six selected tiles can provide a thorough insight into the regional differences between the two datasets and show how topography and

precipitation types affect these two estimates. GPCP 1DD estimates utilize two different algorithms, one for regions equatorward of 40° latitude and second one for regions poleward of 40°. Therefore the analysis of these selected regions (three tiles are above 40°N and three tiles are below 40°N) might reveal the influence of different algorithms on GPCP 1DD estimates. In addition, because precipitation mechanisms vary with season, especially in the CONUS, it is insightful to perform a seasonal analysis. Therefore, comparisons between GPCP 1DD and Q2 estimates were conducted for both the warm season (April – September) and the cold season (October – March) (Wu et al. 2012). Spatial averages were also calculated to study how well the GPCP estimates agree with the Q2 estimates in the spatial pattern of precipitation.

Part II: Evaluation of Reanalyzed Precipitation Data and Trend Analysis

In part II of this study, the evaluation and intercomparison of reanalysis datasets and a trend analysis using GPCP SG monthly data are performed over the CONUS. All comparisons and trend analyses are conducted based on the dataset over a grid box of 1$^\circ \times$ 1° with a total of 957 grid boxes over the study domain. The domain mean precipitation for each year and each month are calculated for GPCP and reanalyses to examine how well the reanalysis can reproduce the year-to-year and month-to-month GPCP SG precipitation patterns. In terms of spatial distribution, annual and seasonal (spring (MAM), summer (JJRA), fall (SON), winter (DJF)) means are calculated to study the regional and seasonal differences between GPCP SG and the reanalyses and among the reanalyses themselves. Furthermore, scatterplots are made between GPCP SG and

reanalyses for domain averaged precipitation over the CONUS each month (a total of 408 months=34 years x 12 months) along with their corresponding linear regression lines. To investigate the differences between GPCP SG and the reanalyses in precipitation distribution, probability distribution functions (PDFs) and cumulative distribution functions (CDFs) are computed from all monthly estimates. Several statistical metrics are also calculated to evaluate the performance of reanalysis datasets such as correlation coefficients, root-mean-square-error (RMSE), and relative difference percentage (RDP %). For trend analysis, a linear regression function is applied to the GPCP SG annual and seasonal accumulated precipitation to generate inter-annual trends by minimizing the chi-squared error. Coefficients of determination are computed for each trend to measure how well the regression line represents the observed precipitation. Finally, the spatial trend distributions of annual and seasonal precipitation over the CONUS during a 34-yr study period are plotted to investigate the regional differences in precipitation trend over the CONUS. Non-parametric Mann-Kendall test (Mann 1945; Kendall 1975) is applied to each grid box to examine if the increasing or decreasing trend is evident.

CHAPTER IV

RESULTS

Part I: Comparison of GPCP 1DD and NMQ Q2 estimates

Comparison of Daily, Monthly, and Yearly Accumulated Precipitation Estimates

Figures 2-4 are scatterplots of daily accumulated precipitation estimates for annual, warm season, and cold season in each tile, respectively, during the period 2010-2012. Each point represents a pair of collocated Q2 and GPCP 1DD daily precipitation estimates (excluding the samples where both GPCP 1DD and Q2 equal
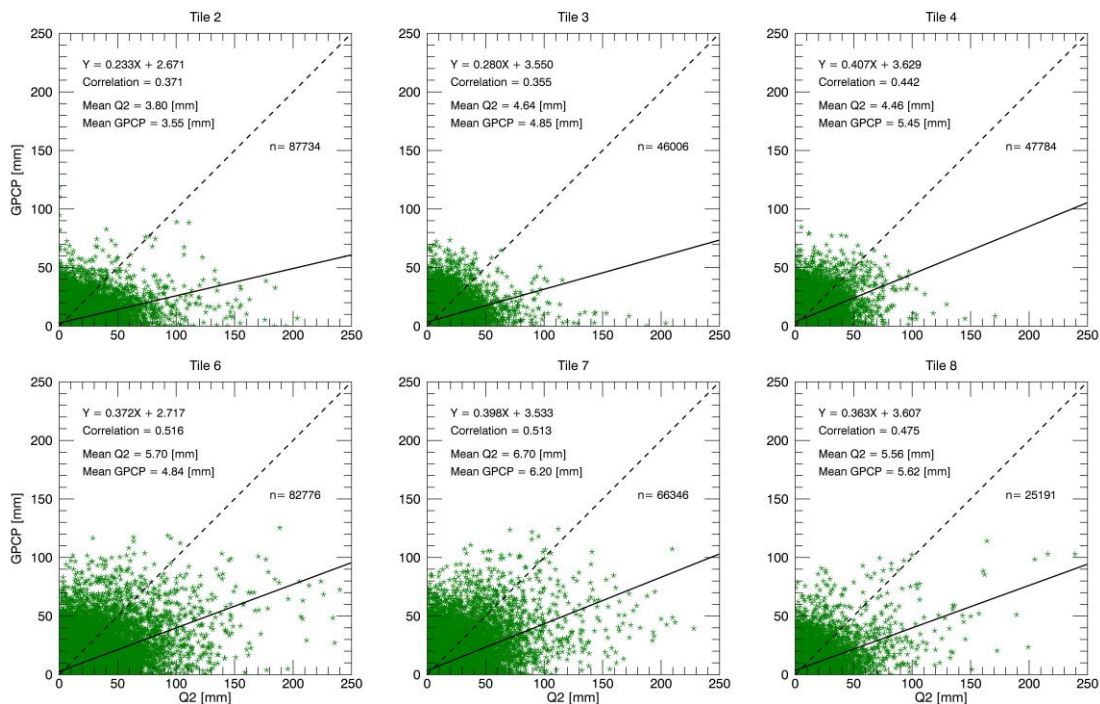
Figure 2. Each point represents a pair of collocated Q2 and GPCP 1DD daily precipitation estimates (excluding the samples for both datasets that equal 0.0 mm) during the period 2010-12 for each tile. The dashed black line is one-one line; the solid line is the linear regression line.

23

0.0 mm). Figure 2 shows that the daily precipitation estimates over the southern tiles (6-8) are generally higher than those over northern tiles (2-4), with the most precipitation falling in tile 7 and the least in tile 2. For the comparisons between Q2 and GPCP 1DD precipitation estimates, the correlation coefficients are slightly higher in southern tiles than in northern tiles, with the highest correlation (0.516) in tile 6 and the lowest (0.355) in tile 3. Q2 estimates exceed GPCP 1DD estimates by 0.25 mm in tile 2, 0.50 mm in tile 7, and 0.86 mm in tile 6, while GPCP 1DD estimates exceed Q2 estimates by 0.21 mm, 0.99 mm, and 0.06 mm in tiles 3, 4 and 8, respectively.

During the warm season, as shown in Fig. 3, daily mean precipitation estimates for both Q2 and GPCP 1DD are higher than annual daily mean precipitation estimates, particularly in tiles 2 and 3, but their correlation coefficients are slightly lower for all tiles except for tile 8, where correlation values are almost the same (0.475 for annual, 0.486 for warm season). Similar to Fig. 2, Fig. 3 shows that the largest negative and positive differences between GPCP 1DD and Q2 precipitation are -1.35 mm in tile 6 and 0.84 mm in tile 4. For tile 8, the difference between GPCP 1DD and Q2 estimates is only 0.2 mm during the warm season, however, GPCP 1DD estimates are 8.1%

24
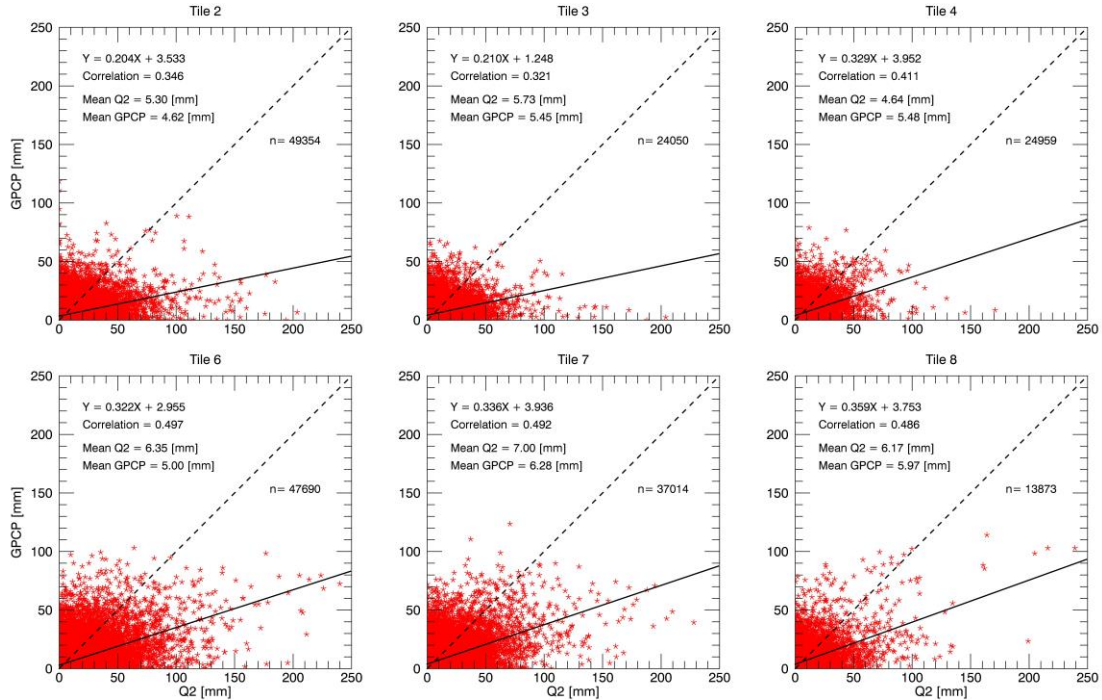
Figure 3. As in Fig. 2, except for the warm season (April-September).

(defined as $\dfrac{GPCP - Q2}{Q2} \times 100\%$) larger than Q2 estimates during the cold season

(Fig. 4). Meanwhile, except for tile 8, slightly higher correlation coefficients are

found between GPCP 1DD estimates and Q2 estimates during the cold season (Fig. 4)

compared to the warm season (Fig. 3). During the cold season, the difference between

two datasets becomes smaller in tile 6 (0.21 mm) but a large difference still exists in

tile 4 with GPCP 1DD estimates larger than Q2 estimates by 1.15 mm. As shown in

these three figures, Q2 daily precipitation is greater than GPCP 1DD estimates in tiles

2, 6, and 7, and lower than GPCP 1DD estimates in tiles 3, 4 and 8 for both warm and

25

cold seasons. The precipitation amounts of northern tiles (2, 3, and 4) are less than their related southern tiles (6, 7, and 8) for annual and warm season. Tile 4 has more precipitation than its related southern tile 8 for cold season. Q2 estimates have more samples with higher precipitation values compared to GPCP 1DD estimates. There are a few samples when GPCP 1DD estimates are around 10 mm while Q2 estimates exceed 100 mm.
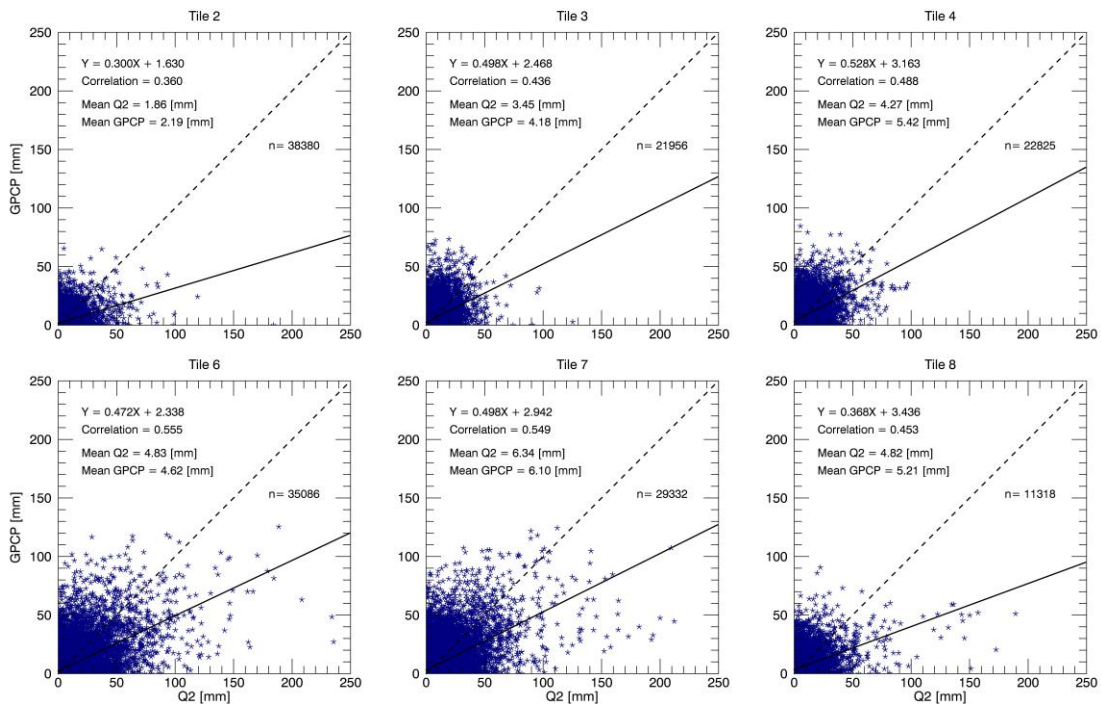
Figure 4. As in Fig. 2, except for the cold season (October-March).

Figure 5 is similar to Fig. 2 except monthly accumulated precipitation from both Q2 and GPCP 1DD daily estimates through the course of a year. Each dot represents a matched pair of Q2 and GPCP 1DD monthly accumulated precipitation. The

26

distributions of Q2 and GPCP 1DD monthly accumulated precipitation and their differences over the six selected tiles in Fig. 5 are very similar to their annual daily counterparts in Fig. 2 except with higher correlation coefficients. Tile 2 has the highest correlation values of 0.855, followed by tile 6, tile 8, and tile 7 with correlation values of 0.819, 0.787 and 0.767 respectively as shown in Fig. 5.
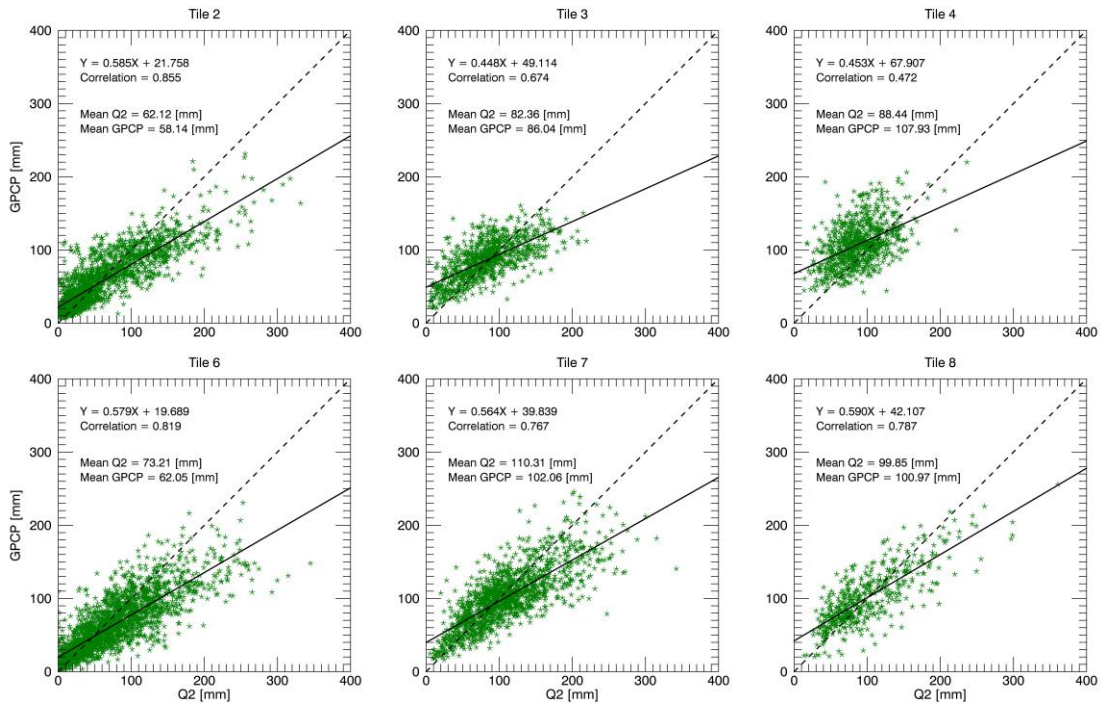
Figure 5. Each point represents a pair of Q2 and GPCP 1DD monthly accumulated precipitation from all of the daily precipitation estimates during a month from 2010 to 2012.

Table 2 presents the mean values and standard deviations for warm and cold seasons' monthly accumulated precipitation estimates of GPCP 1DD and Q2 and their correlation coefficients for each tile. For Q2 estimates, the standard deviations

vary from 29.11 mm (tile 4) to 56.39 mm (tile 6) during the warm season. While

GPCP 1DD estimates have lower standard deviations for each tile range from 20.56

mm (tile 3) to 40.77 mm (tile 8) compared to Q2 estimates. During the cold season,

lower standard deviations are found for both GPCP 1DD and Q2 estimates compared

to the warm season, expect for tile 4 of GPCP 1DD estimates (25.50 for warm season

vs. 31.75 for cold season). Strong correlations are still found in tile 6 for both the

warm (0.760) and cold (0.858) seasons, and weaker correlations are found in tile 4

during the warm season (0.451) and in tile 3 during the cold season (0.418).

Table 2. Mean values (mm) and standard deviations (mm) of monthly accumulated precipitation estimates of Q2 and GPCP 1DD and their correlations for each tile.

		Tile 2	Tile 3	Tile 4	Tile 6	Tile 7	Tile 8
Warm	Q2	97.60	106.34	96.11	93.54	128.43	122.01
	σ	55.28	36.90	29.11	56.39	52.34	55.54
	GPCP 1DD	84.97	101.20	113.36	73.66	115.38	118.00
	σ	32.51	20.56	25.50	37.75	37.94	40.77
	R	0.743	0.514	0.451	0.760	0.687	0.760
	RDP (%)	-12.94	-4.83	17.95	-21.25	-10.16	-3.29
Cold	Q2	26.64	58.37	80.76	52.44	92.18	77.68
	σ	19.90	28.71	30.01	43.82	46.05	35.53
	GPCP 1DD	31.31	70.88	102.50	50.12	88.75	83.94
	σ	17.38	24.39	31.75	35.59	34.45	27.41
	R	0.745	0.418	0.447	0.858	0.797	0.684
	RDP (%)	17.53	21.43	26.92	-4.42	-3.72	8.06

To further investigate the relationship between Q2 and GPCP 1DD estimates,

yearly accumulated precipitation is displayed in Fig. 6. Similar to the monthly
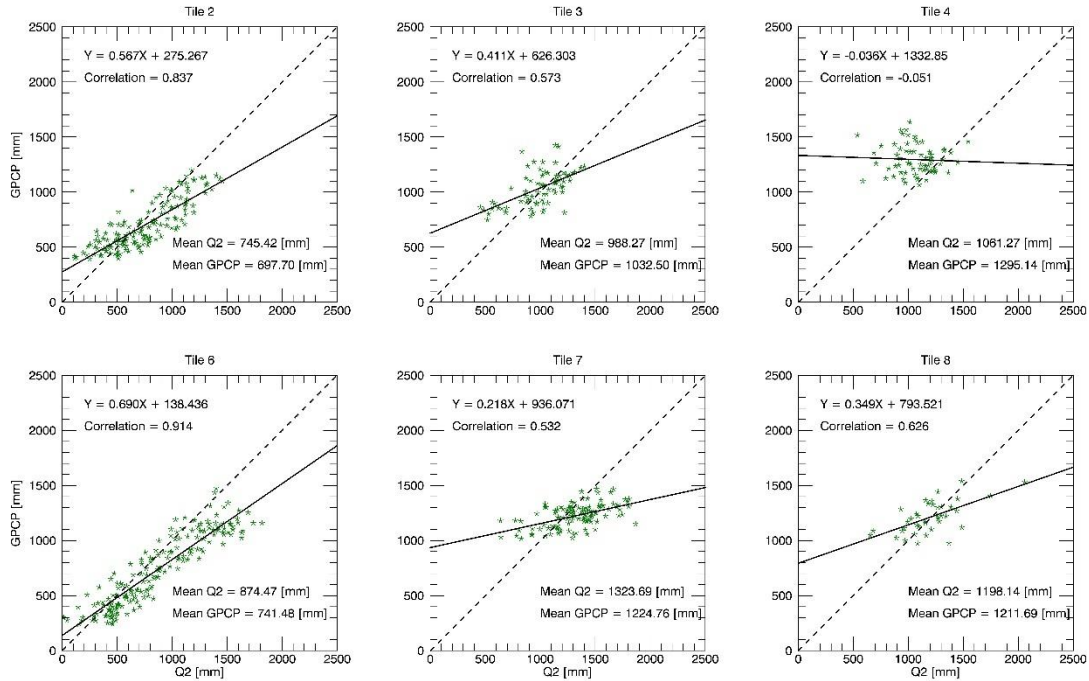
Figure 6. Q2 and GPCP 1DD yearly accumulated precipitation estimates for all 1º × 1º grid points in each tile during the period 2010-12 for each tile.

accumulated precipitation in Fig. 5, each point represents a pair of Q2 and GPCP 1DD yearly accumulated precipitation estimate. As presented in Fig. 6, the least amount of precipitation occurs in tile 2 for both Q2 and GPCP 1DD estimates (745.42 mm and 697.70 mm), while the greatest amount of precipitation is in tile 7 from Q2 estimates (1323.69 mm) and in tile 4 from GPCP 1DD estimates (1295.14 mm). The smallest difference (GPCP-Q2 = 13.55 mm) occurs in tile 8, whereas the largest one (233.87 mm) occurs in tile 4.

Table 3 is similar to Table 2 except for yearly accumulated precipitation

estimates. For the warm season, Q2 estimates vary from 560.54 mm (tile 6) to 770.59 mm (tile 7), and GPCP 1DD estimates have a range from 441.43 mm (tile 6) to 708.02 mm (tile 8). For the cold season, Q2 estimates range from 159.82 mm (tile 2) to 553.10 mm (tile 7), and GPCP 1DD estimates vary from 187.89 mm (tile 2) to 614.97 mm (tile 4). The highest standard deviations occur at tile 6 for both Q2 and GPCP 1DD estimates during warm (311.38 mm for Q2 vs. 211.88 mm for GPCP) and cold (236.55 mm for Q2 vs. 188.07 for GPCP) seasons. Consistent with its daily and monthly comparisons, tile 6 has the highest correlation coefficients (0.914, 0.837, 0.925) for yearly, warm season, and cold season comparisons. Tile 4 has the lowest correlation coefficients for warm and cold seasons. Also for tile 4, the correlation is

Table 3. Mean values (mm) and standard deviations (mm) of yearly accumulated precipitation estimates of Q2 and GPCP 1DD and their correlations for each tile.

		Tile 2	Tile 3	Tile 4	Tile 6	Tile 7	Tile 8
	Q2	585.60	638.04	576.69	560.54	770.59	732.06
	σ	227.83	119.65	114.82	232.45	158.35	182.29
Warm	GPCP 1DD	509.81	607.21	680.17	441.43	692.28	708.02
	σ	134.22	71.44	60.51	153.17	85.96	79.37
	R	0.816	0.417	0.397	0.837	0.473	0.802
	RDP (%)	-12.94	-4.83	17.95	-21.25	-10.16	-3.28
	Q2	159.82	350.23	484.59	313.93	553.10	466.08
	σ	97.20	139.01	112.56	223.28	141.13	119.63
Cold	GPCP 1DD	187.89	425.29	614.97	300.05	532.483	503.67
	σ	82.02	106.67	114.31	179.42	96.96	97.38
	R	0.802	0.536	0.025	0.925	0.647	0.496
	RDP (%)	17.53	21.43	26.92	-4.42	-3.73	8.07

near zero between two datasets in terms of annual accumulated precipitations.

Comparison of Daily Precipitation Occurrence

Figure 7 shows the probability distributions of GPCP 1DD (Q2) daily estimates where Q2 (GPCP 1DD) daily estimates are equal to zero in the six selected tiles. The N0 in Figure 7 represents the total number of daily estimates where both GPCP 1DD and Q2 are equal to 0. While the N1 and N2 represent the total numbers of daily estimates equal to zero for GPCP 1DD and Q2, respectively, during the 3-yr period. Also shown is the percentage of GPCP 1DD (Q2) estimates that are zero given the corresponding Q2 (GPCP 1DD) estimate is equal to zero. For example, in tile 2, with a total of N2=99,231 samples for Q2=0.0 mm, 73.6% of GPCP 1DD samples are equal to 0.0 mm while the other 26.4% GPCP 1DD samples are distributed from 0.0 to 15.0 mm. On the other hand, with a total of N1=94,009 for GPCP 1DD=0.0 mm in tile 2, 77.7% Q2 samples are equal to 0.0 mm while the other 22.3% Q2 samples are distributed from 0.0 to 15.0 mm. The probability distributions for other tiles are similar to those in tile 2, ranging from 70-80% with a maximum co-occurrence ~83% in tile 6. The differences between N1 and N2 for each tile are relatively small, ranging from 1147 (tile 8) to 5222 (tile 2).
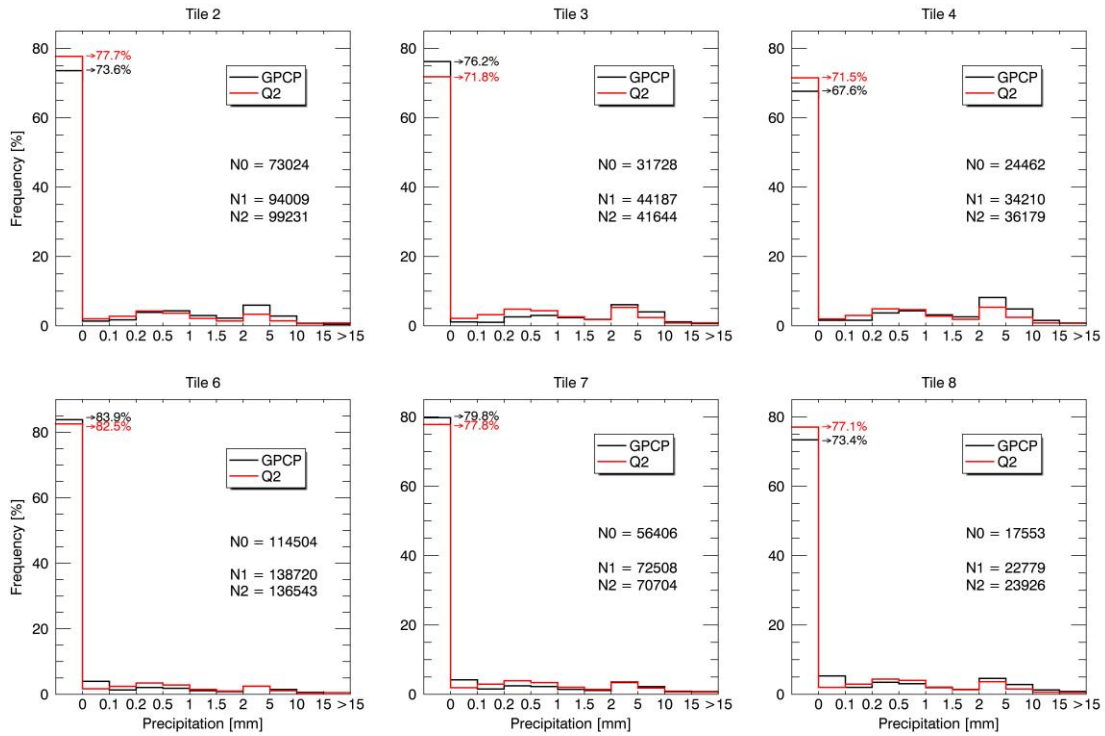
Figure 7. Histograms of GPCP (black) and Q2 (Red) (Q2) daily estimates when daily estimates of the opposite dataset are equal to zero for each tile. N0 represents the total number of daily estimates when both GPCP and Q2 equal to zero. N1 and N2 represent the total numbers of daily estimates equal to zero for GPCP and Q2, respectively. Also shown is the percentage of GPCP (Q2) estimates that are zero given the corresponding Q2 (GPCP) estimate is equal to zero.

Comparison of Regional Precipitation Estimates

Figure 8 presents spatially averaged precipitation from collocated Q2 and GPCP 1DD daily weighted estimates in each tile during the period 2010-2012. The mean precipitation in each tile is calculated from the sum of all daily weighted precipitation estimates (the weighted values are computed based on values used in Fig. 2, i.e., excluding the samples where both Q2 and GPCP 1DD = 0 mm) within the tile, and

then divided by the number of grid boxes. There are a total of 1096 points

(2×365+366) in each tile during the 3-yr period. The mean values of Q2 and GPCP

1DD daily precipitation in Fig. 8 are different to those in Fig. 2 mainly due to the

spatial weighting and spatial averaging. This also results in the slight changes in

relative difference percentage (RDP, defined as $\dfrac{GPCP - Q2}{Q2} \times 100\%$) between the two

datasets. For example, in Fig.2, GPCP 1DD estimates are larger than Q2 estimates by

22.2% for tile 4, whereas this difference is slightly increased to 25.1% in Fig. 8. The
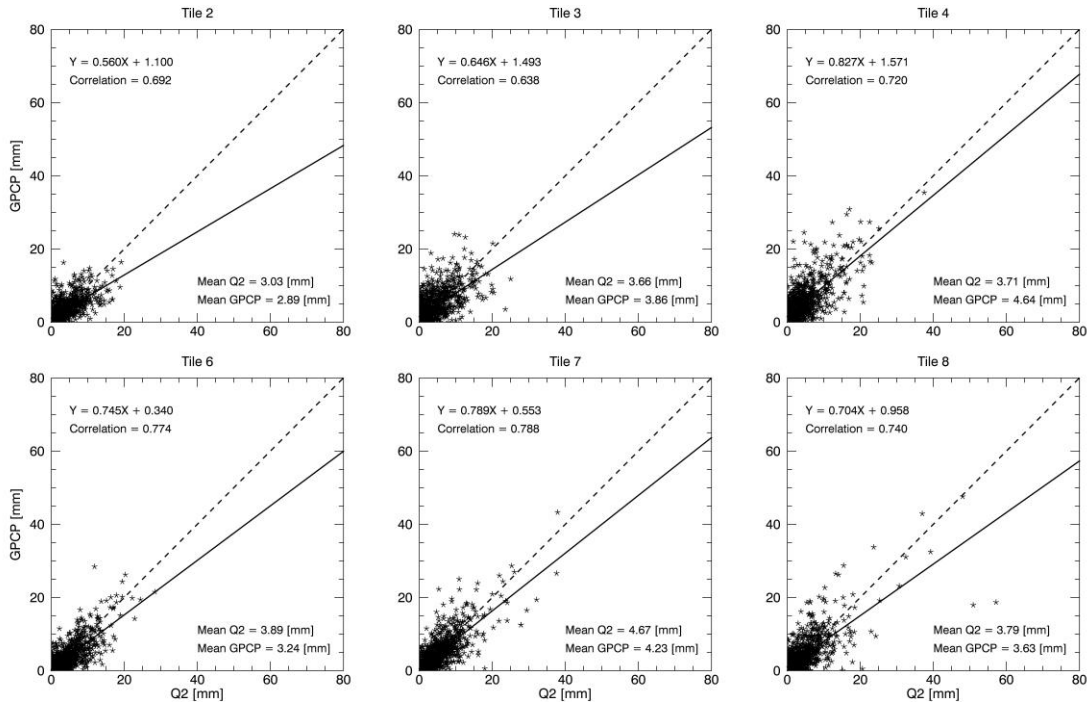
Figure 8. Spatially averaged precipitation from collocated Q2 and GPCP 1DD weighted daily estimates (excluding the samples for both data sets = 0 mm) in each tile during the period 2010-12. Each point represents the mean precipitation in each tile per day.

significant differences between Figures 2 and 8 are much higher correlation

coefficients (0.638-0.788) and stronger linear relationships in Figure 8, indicating that

there are strong correlations for spatially averaged daily precipitation estimates.

Figure 9 is similar to Fig. 8 except that spatially averaged weighted monthly

accumulated precipitation for each tile is shown. Similar to the comparison between

Fig. 2 and Fig. 8, the mean values in Fig. 9 are different from those in Figure 5 due to

the spatially weighting, moreover, very strong correlations found between GPCP
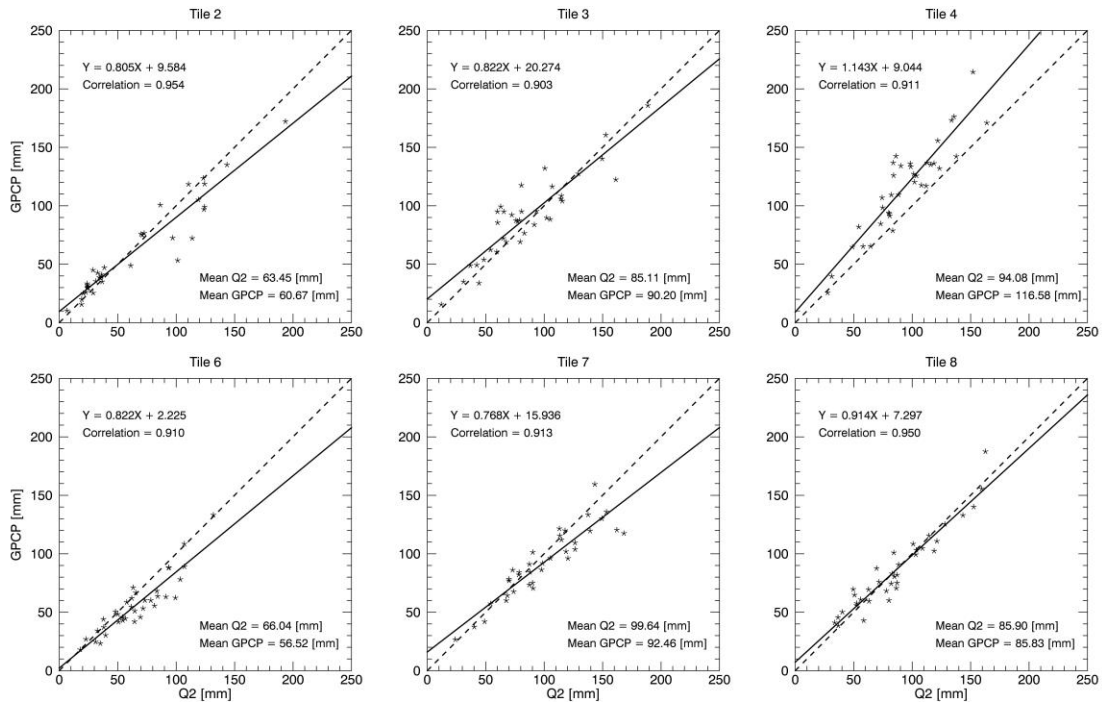
Figure 9. Spatially averaged precipitation from Q2 and GPCP 1DD monthly accumulated precipitation in each tile during the period 2010-2012. Each point represents the spatially averaged (over a tile) monthly accumulated precipitation per month.

34

1DD and Q2 estimates with a range of values from 0.903 in tile 3 to 0.954 in tile 2.

To further investigate the precipitation distributions over the CONUS, the averages of yearly and seasonal accumulated precipitation, as well as their differences (GPCP – Q2) and normalized difference percentages (NDP, defined as $\dfrac{GPCP-Q2}{(GPCP+Q2)/2}\times 100\%$) during the period 2010-2012 are presented in Figures 10 - 12. For the yearly precipitation distribution, GPCP 1DD estimates have a similar pattern to Q2 estimates, with precipitation estimates increasing from west to east over
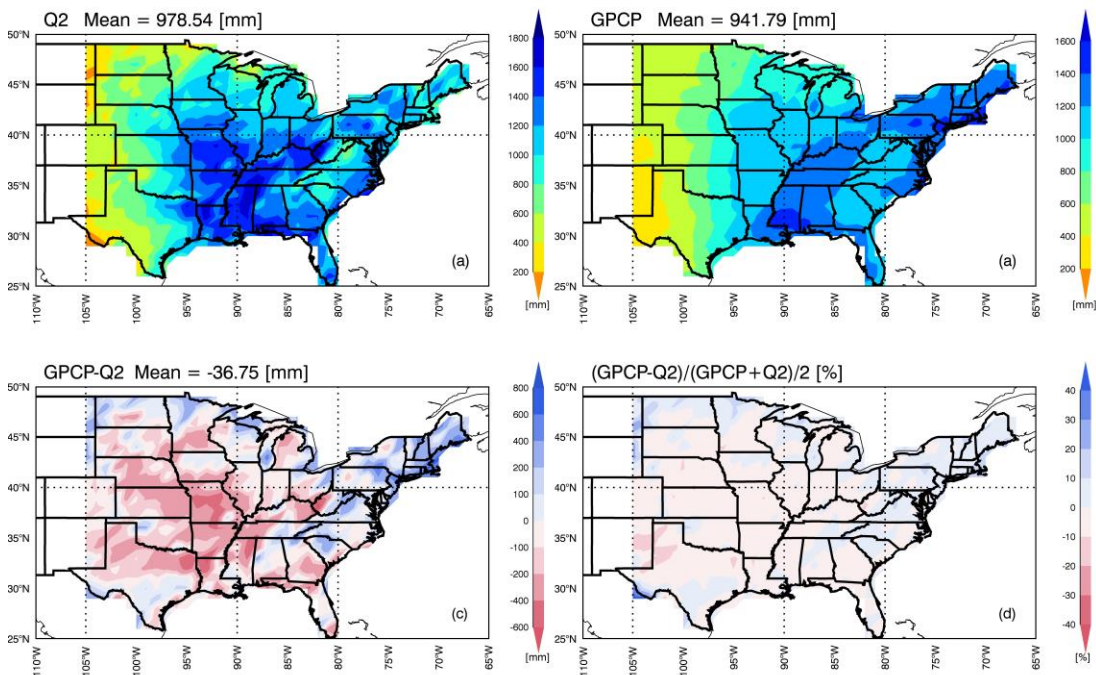
Figure 10. Average yearly precipitation from (a) Q2, (b) GPCP 1DD estimates, (c) their difference (GPCP-Q2), and (d) normalized difference ((GPCP-Q2)/(Q2+GPCP)/2) during the period 2010-2012.

the central U.S., and then decreasing slightly towards the eastern U.S., however, Q2 estimates show more variation than GPCP estimates. Although the difference between their yearly precipitation estimates is only 36.75 mm (3.8%) over the CONUS, there are large regional differences between two datasets. Q2 estimates are much larger than GPCP 1DD estimates over the central US, up to 600 mm larger in GPCP 1DD estimates as illustrated in Fig. 10c. GPCP 1DD estimates are 400 mm less over some areas, while in northern and northeastern regions Q2 estimates are less than GPCP estimates over the Mississippi River Basin, including Missouri, the
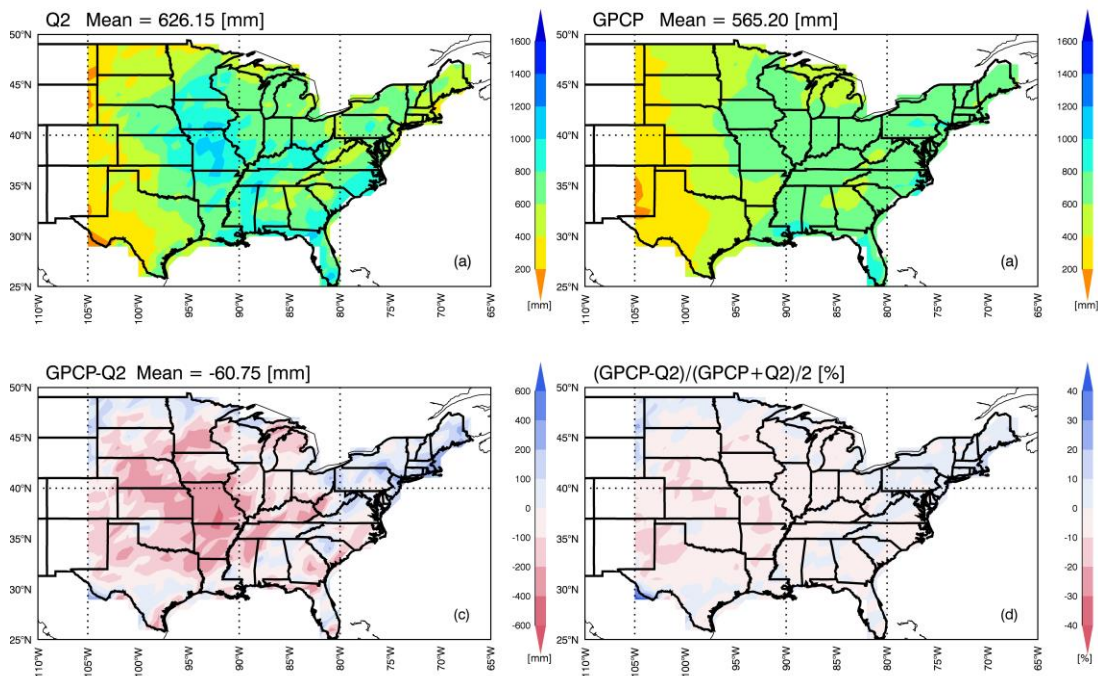
Figure 11. Averaged warm season (April-September) precipitation from (a) Q2, (b) GPCP 1DD estimates, (c) their difference (GPCP-Q2), and (d) their normalized difference ((GPCP-Q2)/(GPCP+Q2)/2) during the period 2010-12.

northeastern corner of Texas to northern Louisiana, northern Mississippi and western West Virginia. The normalized difference percentages (NDP) between GPCP 1DD and Q2 estimates are relatively small with values between -10% to 10% for most of the study region.

Figure 11 shows the distributions of the warm season accumulated precipitation from Q2 and GPCP 1DD, which resembles their yearly precipitation distributions where Q2 estimates vary from 0 to 1200 mm while GPCP estimates have a range of 0 to 1000 mm. GPCP 1DD estimates, on average, are 60.75 mm (NDP=-10.2%) less than Q2 estimates. For the cold season shown in Figure 12, the spatial distribution pattern in Q2 estimates is almost the same as that in the GPCP 1DD estimates with minor differences in some regions. Mean GPCP precipitation is 24.20 mm (NDP=6.6%). larger than mean Q2 precipitation. For some areas over southern Montana and Wyoming, and southwestern Texas, where GPCP 1DD estimates are greater than Q2 estimates by ~100 mm, the NDPs exceed -40% as presented in Fig. 12d. From warm season to cold season, the precipitation amount estimated by Q2 decreased 273.76 mm while GPCP 1DD decreased 188.61 mm.
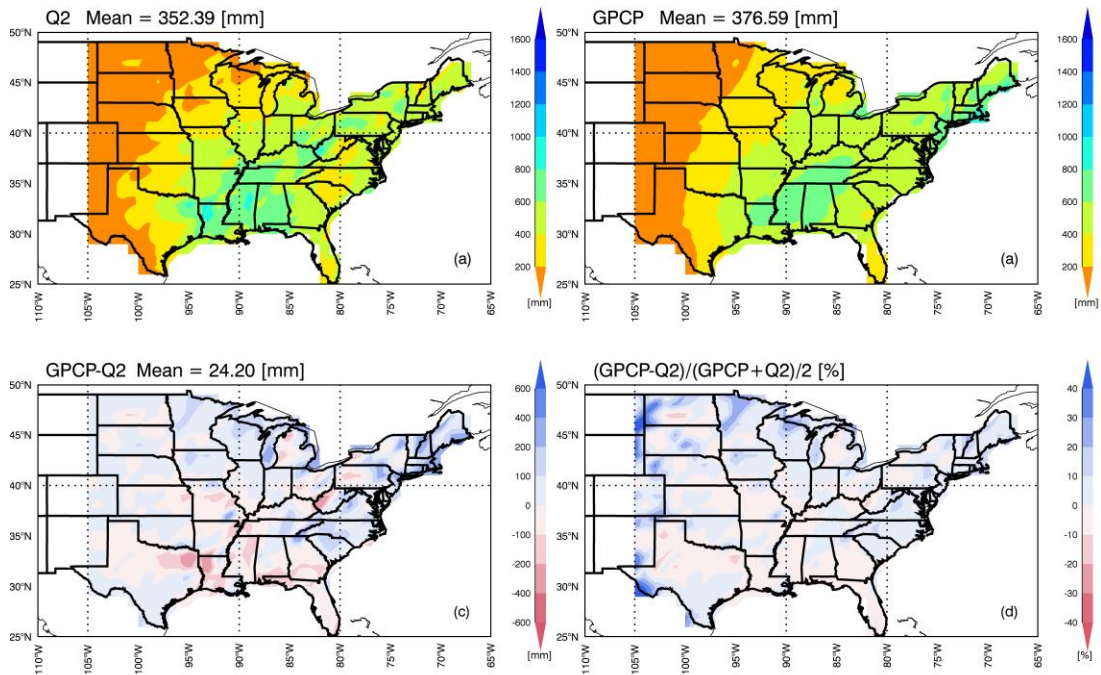
Figure 12. Averaged cold season (October-March) precipitation from (a) Q2, (b) GPCP 1DD estimates, (c) their difference (GPCP-Q2), and (d) their normalized difference ((GPCP-Q2)/(GPCP+Q2)/2) during the period 2010-12.

Part II: Evaluation of Reanalyzed Precipitation Data and Trend Analysis

Evaluation of reanalysis datasets using GPCP SG data

Figure 13 illustrates the spatial distribution of annual mean precipitation of (a) GPCP SG, and (b) – (f) five reanalyses (ERA-I, MERRA2, JRA-55, CFSR, and 20CR) over the CONUS during the period 1980-2013. Fig. 13a shows that the GPCP precipitation amounts generally decrease from the East coast to the West coast with the highest rainfall amounts over the northwest coast, southeast coast, and south central parts of the US while the central west mountain regions receive the lowest. The reanalyses generate similar spatial distributions to the GPCP SG results and capture the variation of the precipitation very well, particularly over the Pacific Northwest regions. However, large differences exist between GPCP SG and the reanalyses over the mountainous areas (approximately between 100° W –120° W) where precipitation amounts predicted by the reanalyses are generally higher than GPCP SG. Most of the GPCP SG precipitation estimates range from 0.25 mm/day to 1.75 mm/day, while all five reanalyzed precipitation amounts can exceed 2.5 mm/day over the mountainous regions. 20CR and JRA-55 also show large areas with discontinuities in precipitation distribution located in the southern part of Montana. For the South-central US (AR, MS, LA), JRA-55, CFSR, and 20CR show similar

features as in GPCP SG whereas ERA-I and MERRA2 predict lower precipitation amounts compared to GPCP SG.
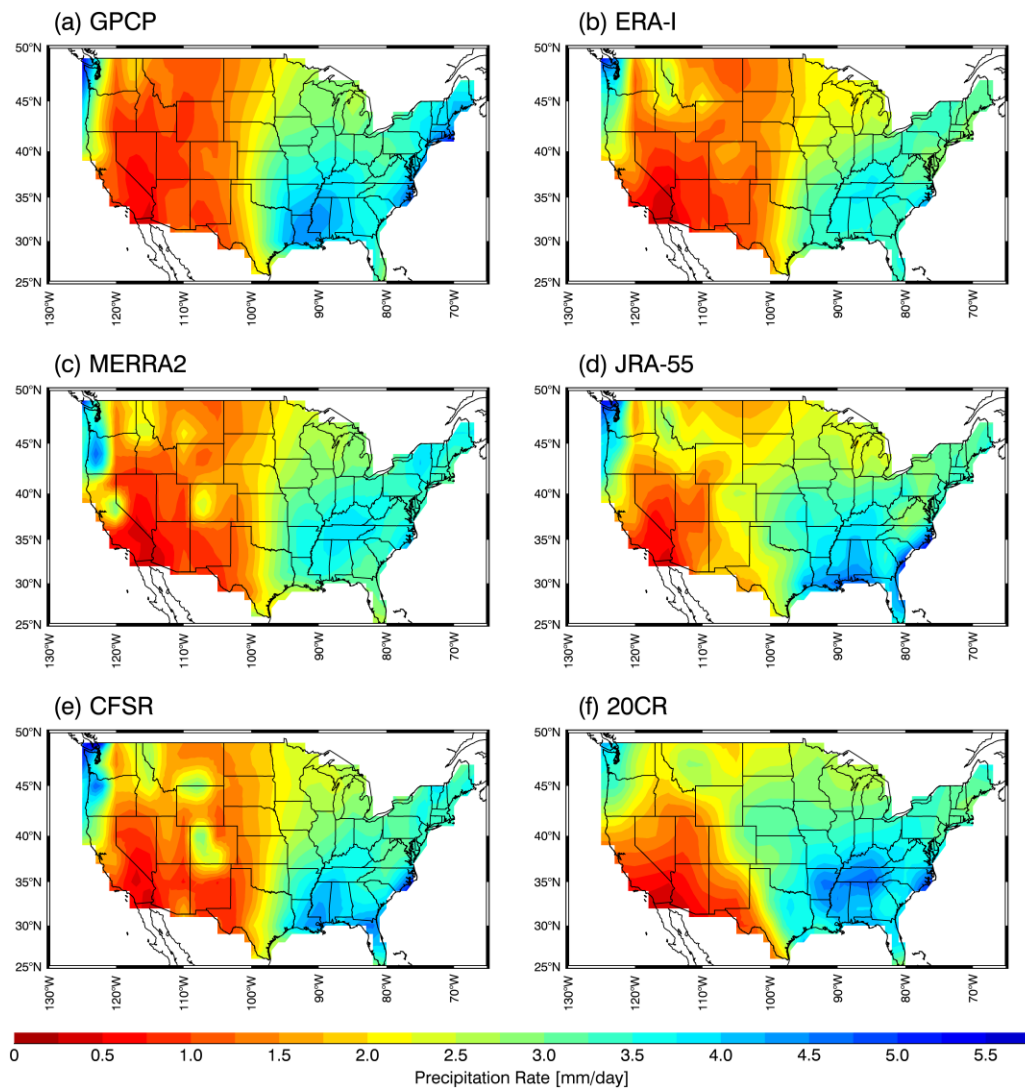
Figure 13. Spatial distribution of annual mean precipitation (mm/day) for (a) GPCP, (b) ERA-Interim, (c) MERRA2, (d) JRA-55, (e) CFSR, and (f) 20CR during the period 1980-2013.

The first row of Fig. 14 shows the GPCP SG's averaged seasonal mean precipitation (spring, summer, fall, and winter) for the period from 1980 through 2013. Rows from two through six show the differences of seasonal mean precipitation in percentage between GPCP SG and ERA-I (second row), MERRA2 (third row), JRA-55 (fourth row), CFSR (fifth row), and 20CR (sixth row). The first row of Fig. 14 shows that high climatological seasonal mean precipitation amounts (first row) are observed by GPCP in the South-central and Northwest regions during the spring. During the summer months, abundant precipitation fall into the southeastern part of the CONUS that the GPCP SG estimated precipitation amounts are greater than 5.0 mm/day. Great Plain regions receive most of its annual precipitation during the summer. From late fall to winter, the precipitation over Northwestern CONUS are generally higher than the rest of the country and the precipitation amount exceeds 5.5 mm/day during the winter as observed in GPCP SG. Meanwhile, the winter precipitation amounts are higher than other three seasons over the northeastern part of the country with precipitation values greater than 4.0 mm/day. The western mountain regions receive the minimum rainfall throughout the year.
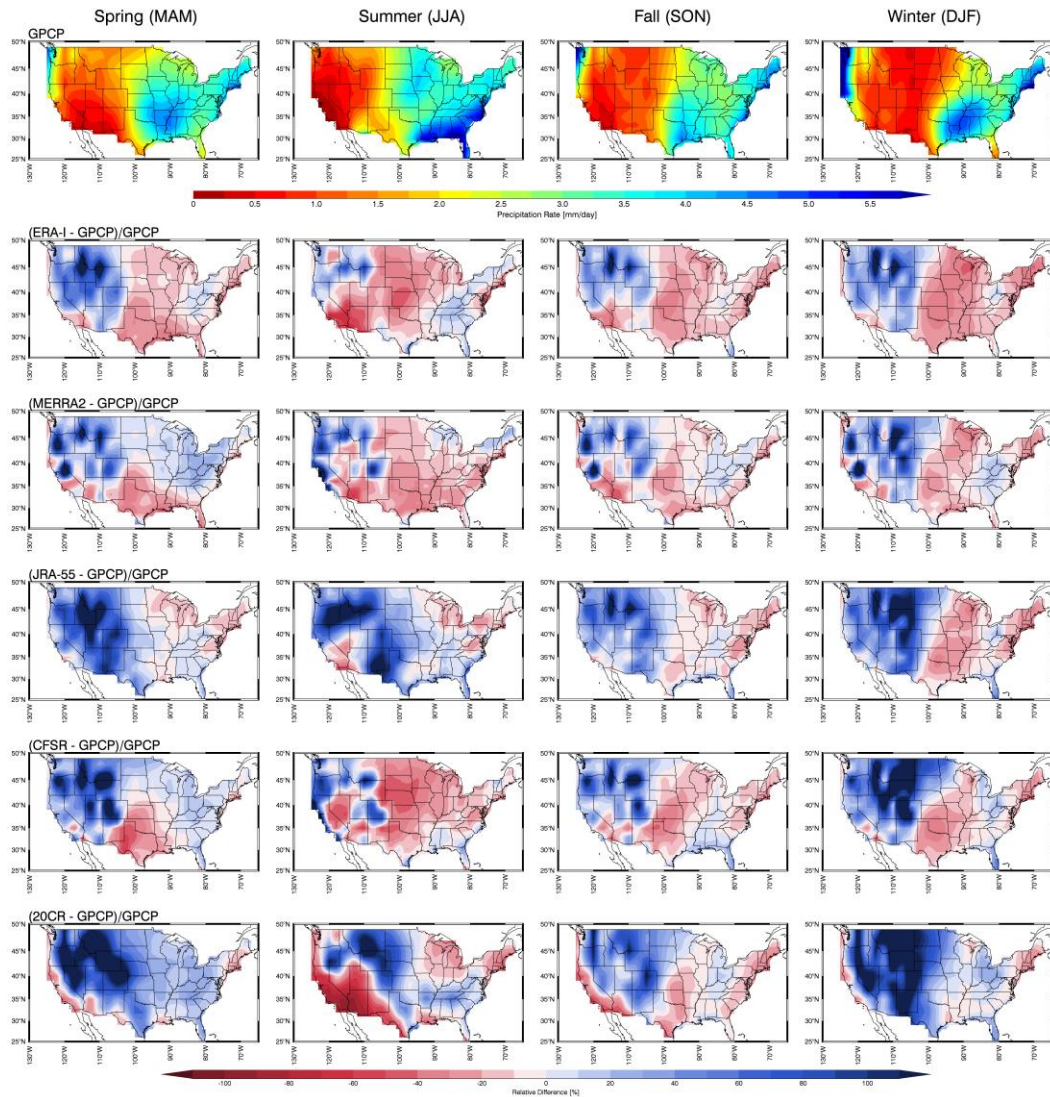
Figure 14. Spatial distribution of seasonal mean precipitation (mm/day) for GPCP (top row) and seasonal relative differences between GPCP and five reanalyses during the period 1980-2013. The columns indicate: Spring (MAM, far left), Summer (JJA, middle left), Fall (SON, middle right), and Winter (DJF, far right).

From rows two through six of Fig 14, the relative difference percentages (RDPs) between GPCP and the reanalyses are defined as

$$RDP = (R - GPCP)/GPCP \times 100\% , \qquad (1)$$

where R represents the precipitation amounts from the reanalyses. Figure 14 has clearly demonstrated that the reanalyzed precipitation amounts are overestimated over the western regions through the course of a year. During spring and winter, the reanalyzed precipitation amounts are as twice as GPCP SG over some parts of Montana, Idaho, and Wyoming. The seasonal spatial distributions of ERA-I, MERRA2 and CFSR are similar to each other in that they underestimate the precipitation amounts over the south-central regions during spring, over the northeast, Great Plains, and southwest during summer, and over the northeast-central regions during fall and winter. The RDP patterns in JRA-55 during fall and winter are similar to the three reanalysis datasets mentioned above, but during spring and summer the underestimated regions of JRA-55 are more concentrated over the Great Lakes and northeast regions. With regard to 20CR, there is a negative bias in the West coast for all seasons, significant underestimation over the southwest region during summer. Differing from the other reanalyses, 20CR severely overestimates the precipitation amounts over the mountain and central regions during spring and winter.

Table 4. Annual and seasonal mean precipitation (mm/day) and standard deviations (in parenthesis) estimated by GPCP SG and the five reanalyses.

	Annual	Spring (MAM)	Summer (JJA)	Fall (SON)	Winter (DJF)
GPCP	2.38 (1.89)	2.40 (1.75)	2.61 (1.89)	2.31 (1.91)	2.22 (2.00)
ERA-I	2.16 (1.67)	2.28 (1.48)	2.34 (1.85)	2.08 (1.65)	1.96 (1.67)
MERRA2	2.29 (1.83)	2.49 (1.78)	2.29 (1.80)	2.01 (1.84)	2.16 (1.88)
JRA-55	2.61 (1.87)	2.70 (1.63)	3.07 (2.07)	2.40 (1.86)	2.25 (1.80)
CFSR	2.38 (1.88)	2.59 (1.69)	2.28 (2.03)	2.30 (1.93)	2.34 (1.82)
20CR	2.68 (1.92)	3.11 (1.88)	2.72 (2.25)	2.30 (1.73)	2.60 (1.70)

The seasonal mean precipitation amounts (mm/day) and their standard deviations estimated by GPCP SG and five reanalyses are shown in Table 4. GPCP SG has annual mean precipitation of 2.38 mm/day and a standard deviation of 1.89 mm/day. CFSR has the same annual mean as GPCP SG and closest standard deviation among reanalyses (1.88 mm/day vs 1.89 mm/day) among all the reanalysis datasets. The seasonal mean precipitation of GPCP SG ranges from 2.22 mm/day during winter to 2.61 mm/day during summer. The highest standard deviation of 2.00 mm/day occurs during winter and is likely because of the large precipitation amounts in the northwest region that increases the variation of precipitation values in GPCP SG. Other than MERRA2, which has its highest standard deviation during winter, the highest standard deviations for the other reanalyses occurred during summer. Table 5 provides the RMSEs (first row) and RDPs (second row) of seasonal mean precipitation for

each reanalysis using GPCP SG as reference. The RDPs are calculated using the spatially integrated mean values instead of averaging the RDPs from each grid box. On average, ERA-I underestimates the annual precipitation by ~9%, and the negative biases of ERA-I are observed throughout the year. Nonetheless, the RMSEs of ERA-I for each season are the smallest among the five reanalyses. On the contrary, JRA-55 overestimates the precipitation for all seasons, especially during summer, with a RDP of ~17%. MERRA2 and CFSR show lower biases, except they significantly underestimate the summer precipitation with RDPs greater than 12%. 20CR has positive biases for all seasons except for fall, particularly during spring when 20CR is ~29% higher than GPCP SG. 20CR also has the highest RMSE during each season.

Table 5. RMSE (first row) and relative differences in percentage (second row) of five reanalyses using GPCP SG as a reference.

	Year around	Spring (MAM)	Summer (JJA)	Fall (SON)	Winter (DJF)
ERA-I	0.95	0.90	1.05	0.92	0.93
	-9.2%	-5.0%	-10.3%	-10.0%	-11.7%
MERRA2	1.01	0.99	1.11	0.94	0.97
	-3.8%	3.8%	-12.3%	-13.0%	-2.7%
JRA-55	1.07	1.00	1.28	1.00	0.98
	9.7%	12.5%	17.6%	3.9%	1.4%
CFSR	1.14	1.09	1.35	1.07	1.01
	0.0%	7.9%	-12.6%	-0.4%	5.4%
20CR	1.34	1.40	1.63	1.20	1.08
	12.6%	29.6%	4.2%	-0.4%	17.1%

45

To further examine the performance of the reanalysis datasets, the correlation coefficients of monthly precipitation amounts between reanalyses and GPCP SG are calculated from 1980 through 2013 for each grid box and are presented in Fig. 15. The spatial distributions of correlation coefficients have illustrated that all reanalyses are in excellent agreement with GPCP SG over the western part of the US, where the correlation coefficients exceed 0.9. For the central to eastern parts of the country, MERRA2 is well correlated with GPCP SG, with most of the study region having correlation coefficients greater than 0.8. For ERA-I and JRA-55, the correlations are less than 0.7 over the north to central mountain regions, which corresponds to the regions where ERA-I and JRA-55 largely overestimate precipitation as shown in Fig. 14. For CFSR, the correlations are between 0.65 and 0.8 for the central and east regions. 20CR is less correlated with GPCP SG with respect to other reanalyses. Lower correlations around 0.2 to 0.35 are found between GPCP and 20CR over the eastern Arizona to western New Mexico.
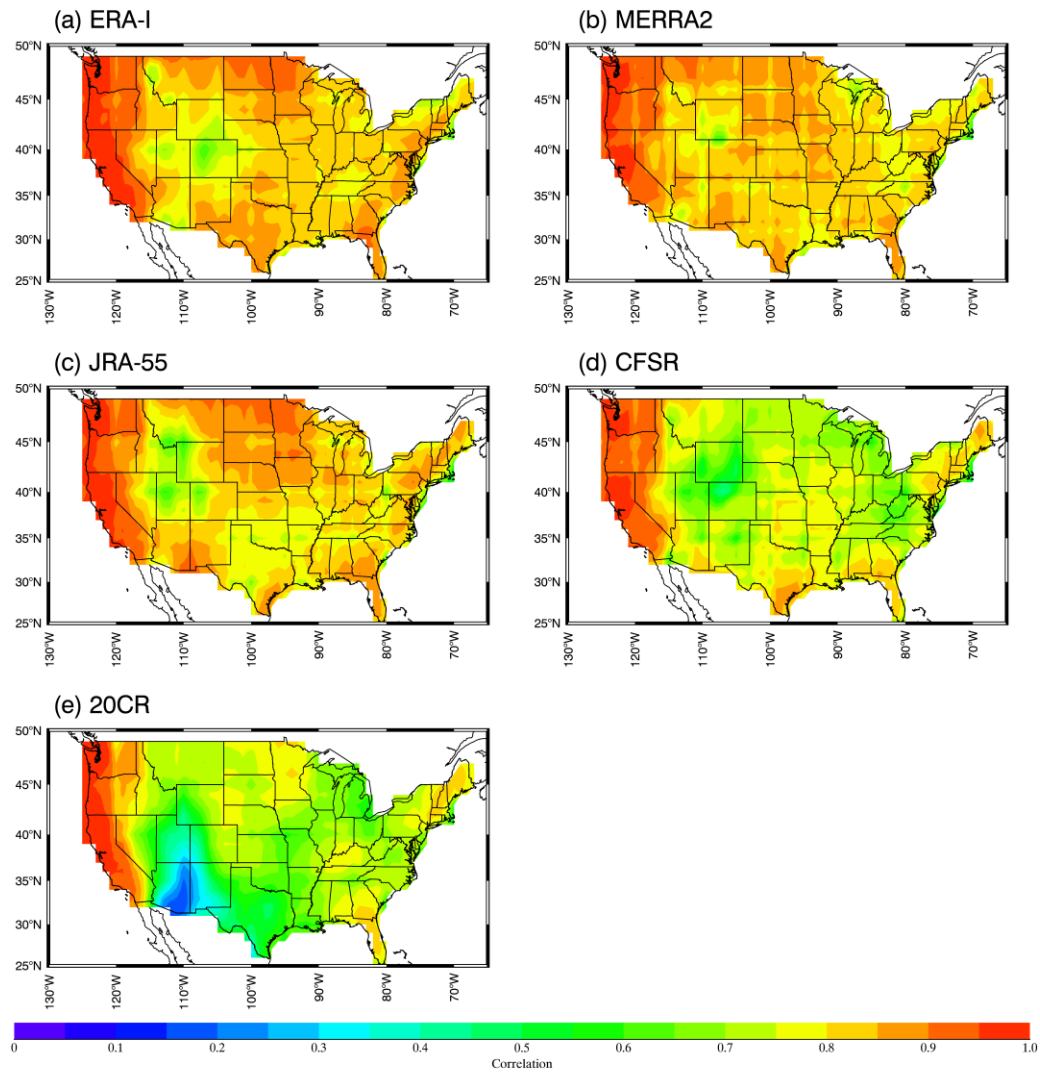
Figure 15. Spatial distribution of correlation coefficients between GPCP SG and five reanalyses during the period 1980-2013.

Figure 16 shows the time series of (a) annual mean precipitation averaged over the CONUS (mm/day) and their (b) anomalies (mm/day) from GPCP SG and reanalyses from 1980 through 2013. Although the reanalyses exhibit similar
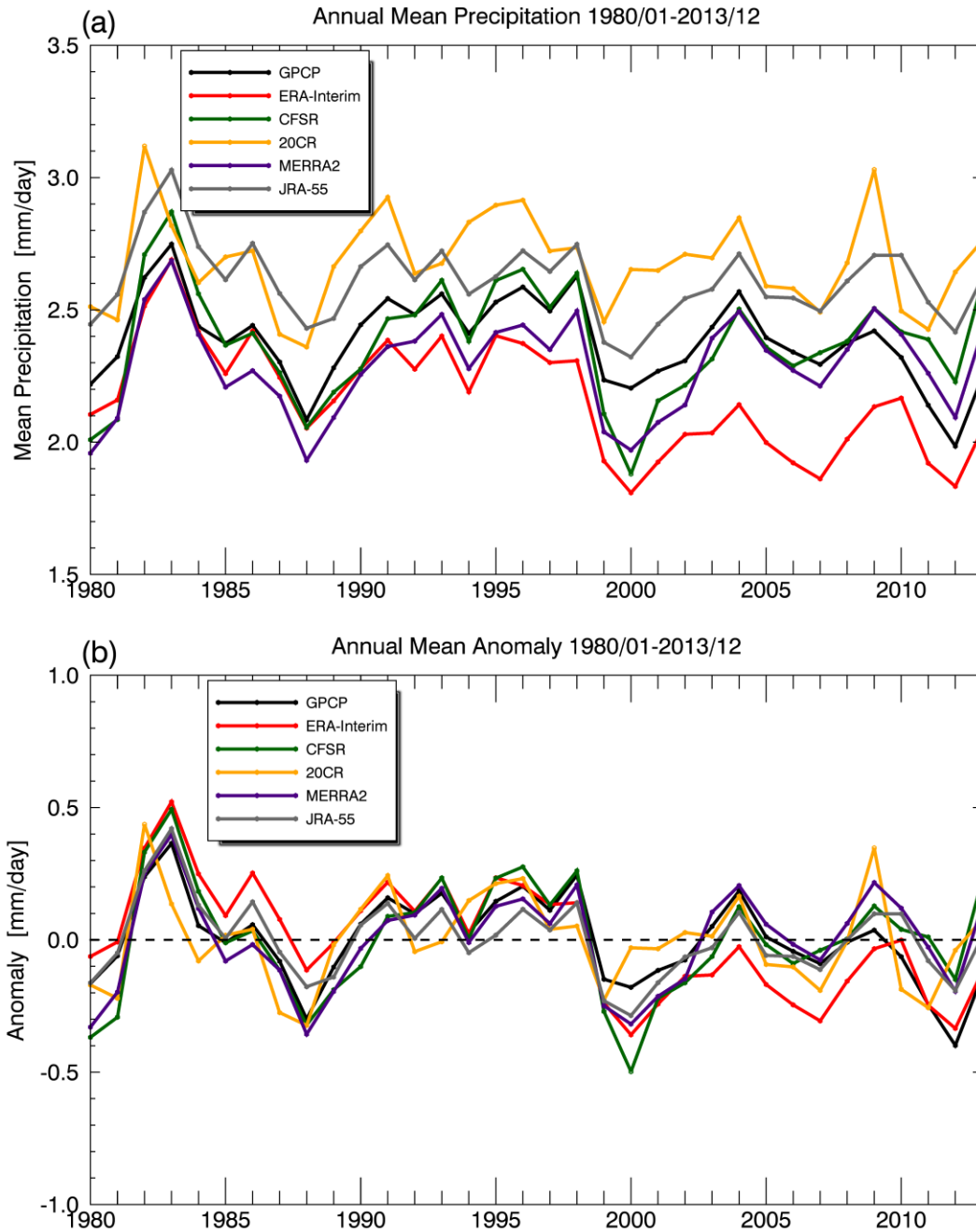
Figure 16. (a) Annual average precipitation (mm/day) for GPCP SG and five reanalyses and (b) their respective anomalies from 1980 through 2013.

inter-annual variability and trend of precipitation to GPCP SG over the CONUS, their magnitudes are significantly different. During the study period, 20CR (yellow line) and JRA-55 (grey line) have constant positive biases while ERA-I (red line) shows constant negative biases compared to GPCP (black line). MERRA2 (purple line) and CFSR (green line) have precipitation nearer to GPCP, and CFSR shows almost identical precipitation values as GPCP during the periods from 1985 to 1988, and from 1997 to 1999. Their annual precipitation anomalies are given by the annual mean precipitation for that year minus the climatological mean precipitation during the period 1980-2013. Except for 20CR, the anomaly patterns of the reanalyses are in good agreement with GPCP SG and well capture the inter-annual variations. For instance, GPCP SG, ERA-I, CFSR, MERRA2, and JRA-55 have highest positive anomaly at year 1983, but 20CR does not catch this feature and the trend of 20CR shifts from other datasets.

To investigate the seasonal variations, the mean precipitation for each month is calculated from 1980 to 2013 as displayed in Fig. 17. The monthly mean precipitation monotonically increases from January to June, reaches the maximum in June, and then generally decreases through the following months to December as observed in
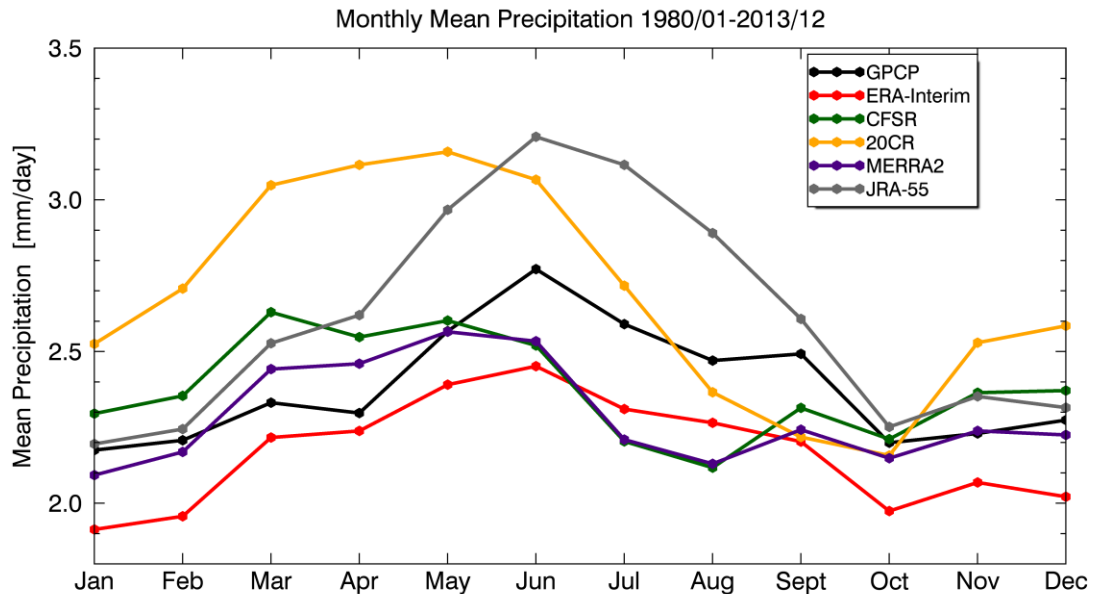
Figure 17. Monthly mean precipitation (mm/day) for GPCP SG and five reanalyses during the period 1980-2013.

GPCP SG. JRA-55 and ERA-I show similar seasonal variations to GPCP SG but JRA-55 overestimates the precipitation values, particularly during the warm season months, while ERA-I underestimates the precipitation throughout the year. Both MERRA2 and CFSR overestimate precipitation from January to May, peak in March, but greatly underestimate precipitation from June to September. In contradiction to others, 20CR shows a somewhat unreasonable seasonal variation with decreasing precipitation amount from May to October and then increasing from October to following May.

Histograms of the probability distribution functions (PDFs) and cumulative

distribution functions (CDFs) of monthly mean precipitation from GPCP SG (blue line in each plot) and five reanalyses (red line in each plot) are plotted in Fig. 18 (a total of 957 grid boxes×408 months). The median precipitation values of GPCP SG (blue) and reanalyses (red) are presented in Fig. 18. Both ERA-I and MERRA2 have similar number of light precipitation events (< 1.0 mm/day) as GPCP SG, but there are more estimates with precipitation values between 1.0 to 3.0 mm/day and less estimates between 3.0 to 8.0 mm/day (i.e., more skewed). The percentages of JRA-55 and 20CR reanalyzed precipitation amounts that are less than 1 mm/day are around 20%, which is ~8% less than the GPCP SG estimates. Their PDFs are more skewed to higher precipitation values, especially for 20CR; therefore, the median of 20CR is much higher than GPCP SG (2.39 mm/day vs. 1.99 mm/day). This is likely the result of a relatively coarse spatial resolution (2°× 2° for 20CR, and 1.25°× 1.25° for JRA-55), making it difficult to capture light and localized precipitation events. Except few percent differences for estimates between 0 to 3.0 mm/day, the PDFs of CFSR mimic the PDFs of GPCP SG. Unexpectedly, the total number of high precipitation analyses (> 8.0 mm/day) of all reanalyses agrees well with GPCP, but it may due to the small number of samples.
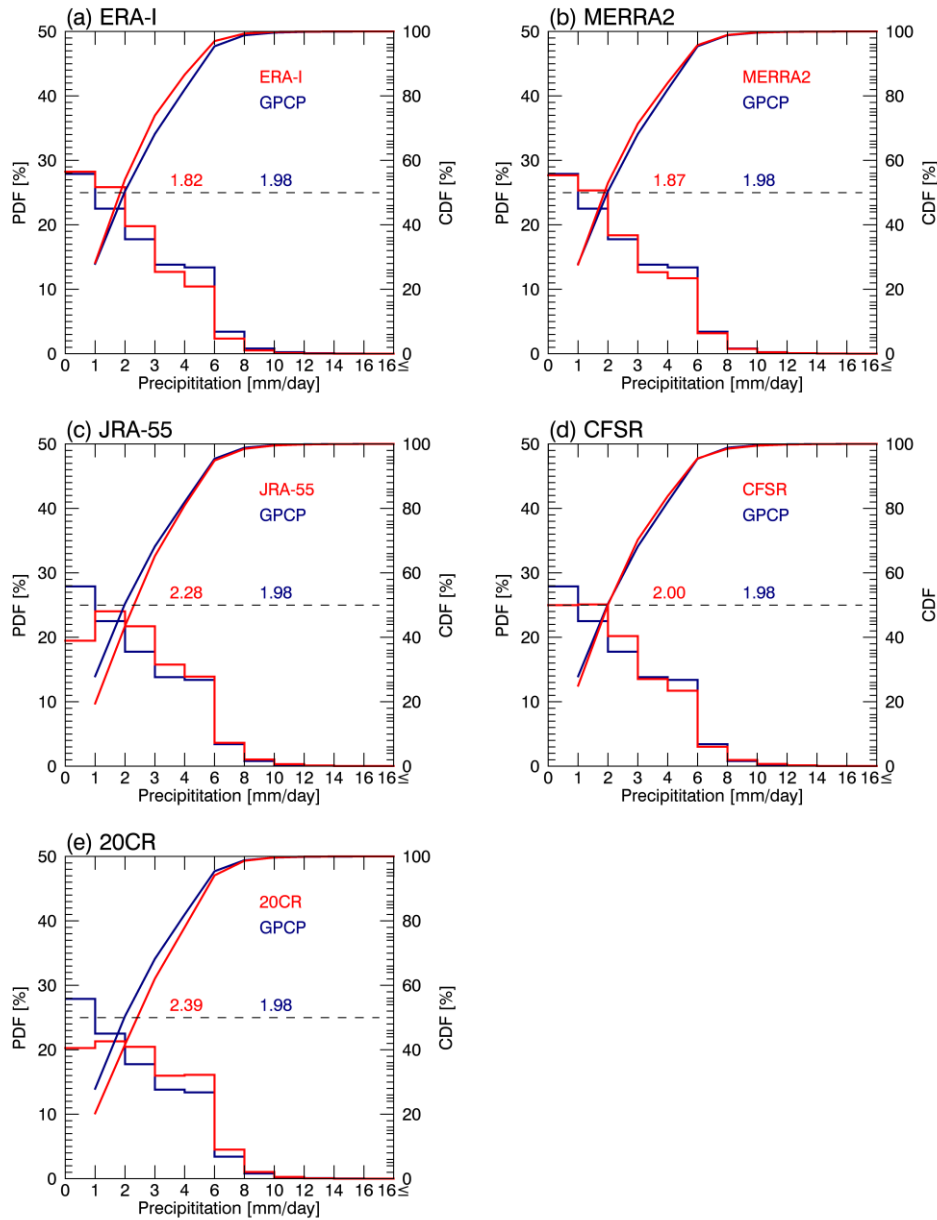
Figure 18. Probability Distribution Functions (PDFs) (%) and Cumulative Distribution Functions (CDFs) (%) for GPCP SG (blue) and five reanalyses (red) of monthly mean precipitation (mm/day) (a total of 951 grid boxes×408 months). Dash line represents the median line (50%). The values listed in the plots are the median monthly mean precipitation of GPCP SG (blue) and reanalyses (red).

The scatterplots of the monthly spatially-averaged precipitation within the CONUS are presented in Fig. 19. GPCP SG is on the x-axis, and the reanalysis product is on the y-axis. Also shown are the correlation coefficient and RMSE between GPCP SG and the reanalysis, and their linear regression function. From the plot, strong linear relationships and good agreement are found between GPCP SG and all reanalyses with correlation coefficients ranging from 0.697 for 20CR to 0.892 for JRA-55. These results indicate that reanalyses can represent the spatial pattern of GPCP SG reasonably well. Compared to the values in Table 5, smaller RMSEs are observed between GPCP and the reanalyses, varying from 0.243 mm/day for MERRA2 to 0.490 mm/day for 20CR, which is due to the large domain spatial averaging.

To further evaluate the performance of reanalyzed precipitation estimates with GPCP SG, Taylor diagram has been generated in Fig. 20. The standard deviation is defined as the standard deviation of the ratio of the reanalysis precipitation amount to GPCP SG precipitation amount, which shows the amplitude of the variation of reanalysis with respect to GPCP SG. Both correlation coefficient and standard deviation are calculated using monthly mean precipitation during the period 1980-2013. For each season, all reanalysis datasets are well correlated with GPCP SG
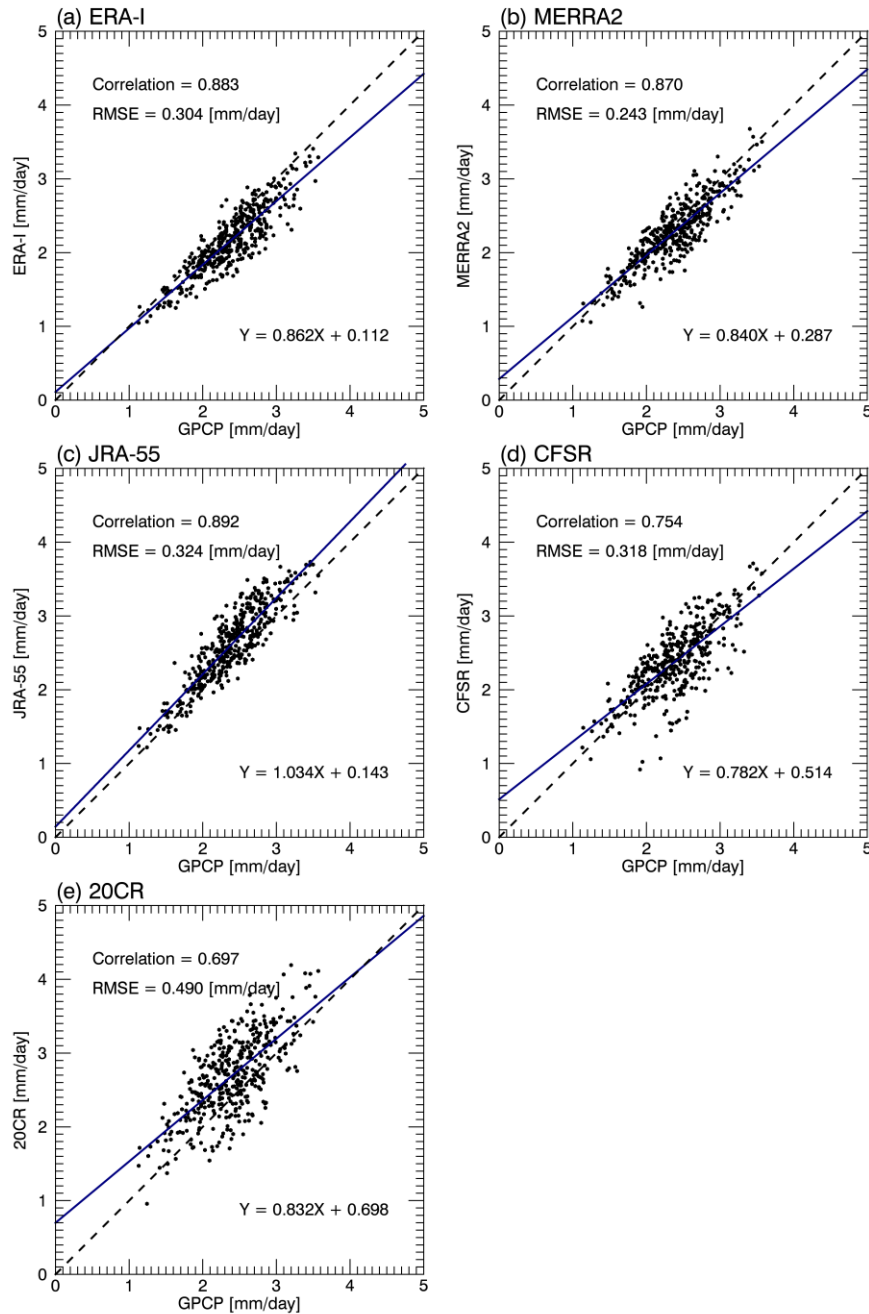
Figure 19. Scatterplots of GPCP SG and each reanalyses domain averaged monthly mean precipitation over the CONUS (a total of 408 dots=34 years X 12 months), and their correlation coefficient, RMSE with their linear regression line.

(correlation coefficients > 0.7). The standard deviations are higher during summer, particular in CFSR and MERRA2. The standard deviation of 20CR is high during the fall, which is around 2.5. JRA-55 shows the least seasonal variations, with comparatively constant correlations between 0.8 to 0.88 and standard deviations around 1.2.
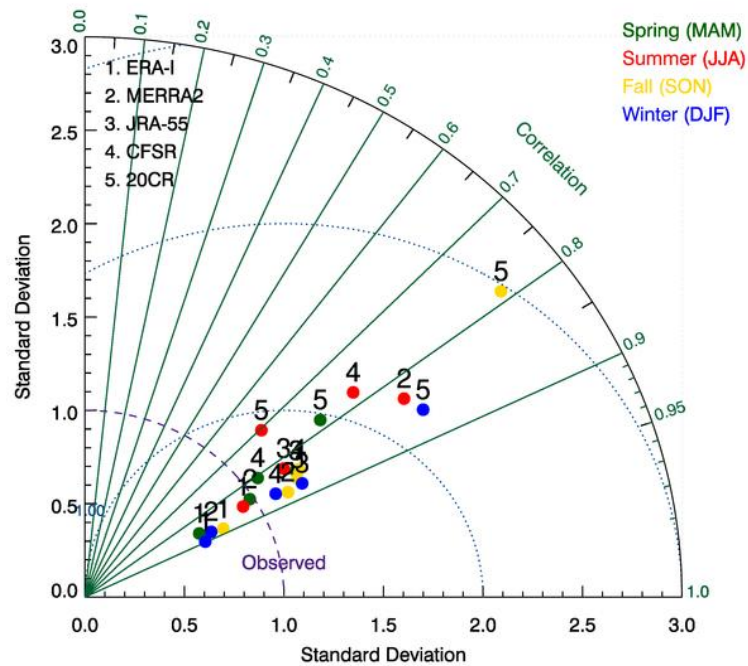
Figure 20. Taylor diagram for the correlations and standard deviations of seasonal precipitation from five reanalyses using GPCP SG as a reference. Each point shown on the plot is calculated based on a total of 957 grid boxes×102 months (99 months for winter).

Trend Analysis

To perform a long-term trend analysis, a homogeneous dataset should be used to represent the nature of precipitation variation. Because GPCP product incorporates the satellite observations, it should be noted that changes in the input data sources might lead to inhomogeneity in GPCP product and could result in the false trending. For example, the GPCP precipitation estimates were primarily from the OPI estimates during the period 1979-1986, thereafter, the GPI estimates calibrated by SSM/I data were used (Adler et al. 2003). Efforts have been made to minimize the inhomogeneous in GPCP from the original to current version. Additional adjustments using gauge data have been applied to OPI estimates during the pre-SSM/I period (Huffman and Bolvin 2013) to reduce the inconsistences brought by the transition between OPI and GPI estimates and the inclusion of SSM/I data. Before Version 2.1, the gauge analyses used in GPCP were from the Global Historical Climate Network and Climate Analysis and Monitoring System (GHCN + CAMS) during the period 1979-1985, and GPCC gauge data thereafter. Starting with Version 2.1, the entire GPCP gauge analysis field (1979-present) is reprocessed with the upgraded GPCC gauge analysis with much higher number of gauges (Huffman et al. 2009). This change benefits the precipitation estimates over land, particularly for the regions with

good coverage of GPCC network, such as the CONUS. Gruber and Levizzani (2008) examined the changes in global precipitation from GPCP Version 2 during the pre-SSM/I (1979-1986) and SSM/I (1988-2003) periods. The results showed that the overall spatial distributions of precipitation for these two periods have great similarities, except for slightly lower values in the mid-latitudes over land and slightly higher values in the tropics during the period 1988-2013. Note that over the CONUS, the differences between two periods are within a range from -0.5 to -0.2 mm/day. Huffman et al. (2009) also investigated the influences of the input data by computing the linear rate of change in precipitation for both GPCP Version 2 and Version 2.1 during the entire period (1979-2007) and SSM/I period (1988-2007). Because Version 2.1 is driven by the GPCC gauge data and focuses more over the land, the rate of change for global land shifts from +0.0018 mm day^{-1} decade^{-1} in Version 2 to -0.0118 mm day^{-1} decade^{-1} in Version 2.1 during the period1979-2007. As for SSM/I period, the linear rate over global land decreases from +0.0630 to +0.0252 mm day^{-1} decade^{-1} from Version 2 to Version 2.1. Over the CONUS, the linear changes range from -0.3 to -0.1 mm day^{-1} decade^{-1} over the western part of the country. Consequently, a decreasing precipitation trend over the CONUS should be expected using the current version of GPCP.

Figure 21 shows the inter-annual variabilities of GPCP SG annual and seasonal accumulated precipitation over the CONUS during the 34-yr study period. The blue line represents the linear regression fit to the accumulated precipitation by minimizing the chi-square error. The shaded areas contain the precipitation values within the 95% confidence level, which are calculated based on the student-t test. Numbers shown are the slope of the regression line and the coefficient of determination (denoted as R^2) between GPCP SG precipitation estimates and
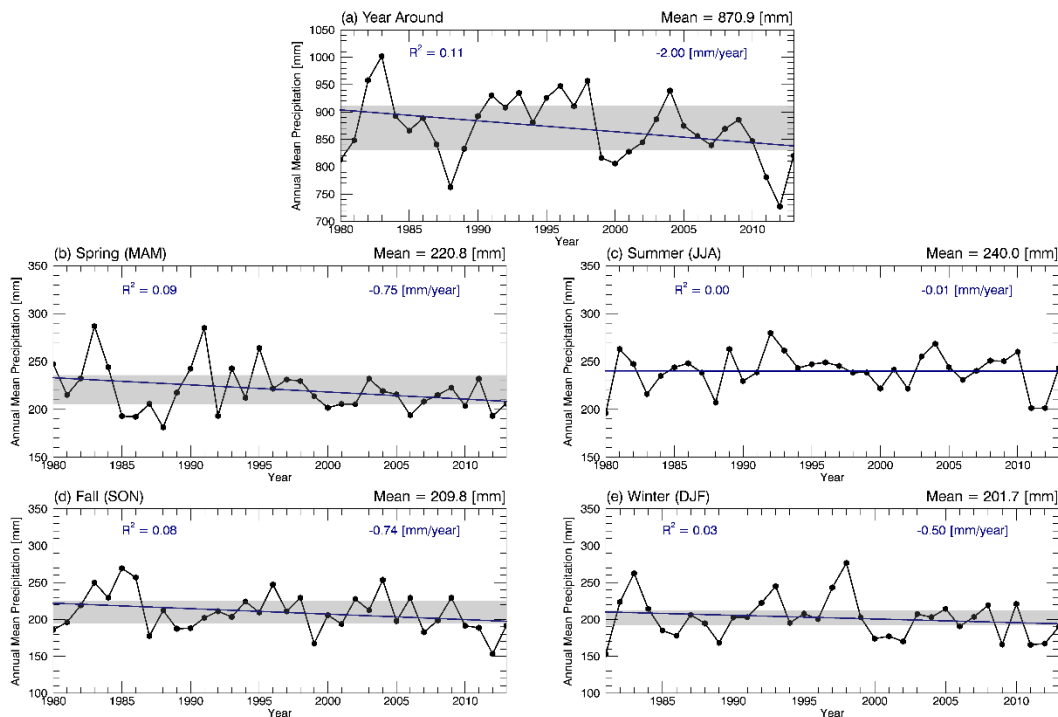
Figure 21. (a) Annual and (b-e) seasonal accumulated precipitation (mm) estimated by GPCP SG and their linear trends (red line) during the period 1980-2013. The shaded areas represent the area within 95% confidence interval of the slope (based on the student t-test).

58

calculated values by the regression line. GPCP SG has an annual average precipitation of 870.9 mm over the 34-yr period. According to the regression line, the annual precipitation amounts decreased 2.0 mm/yr from 1980 to 2013. This decreasing trend is also observed during four seasons with the minimum decreasing rate of -0.01 mm/yr during summer and the maximum rate of -0.75 mm/yr during spring. The variation of inter-annual precipitation is large from 1980 to 2013 with R^2 values near zero and more than 17 years of samples outside of 95% confidence interval range for year around as well as seasonal precipitation. The annual accumulated precipitation amounts are extremely high in 1983 (1002.0 mm), and lows in 1988 (762.6 mm) and 2012 (727.4 mm).

In addition to temporal trend analysis, a trend analysis of spatial distribution is conducted for annual and seasonal GPCP SG precipitation shown in Fig. 22. Based on a total 34 years of data, the precipitation trend is calculated at each grid box using the same linear regression method as above. Furthermore, Mann-Kendall test is used to determine if the grid box has an increasing or decreasing trend which is significant at the 95% confidence interval. For the grid box having evident trend are marked as a cross on Fig. 22. For annual trend, the northeastern and north-central parts of the country show positive trends, while other regions show negative trends in annual

59
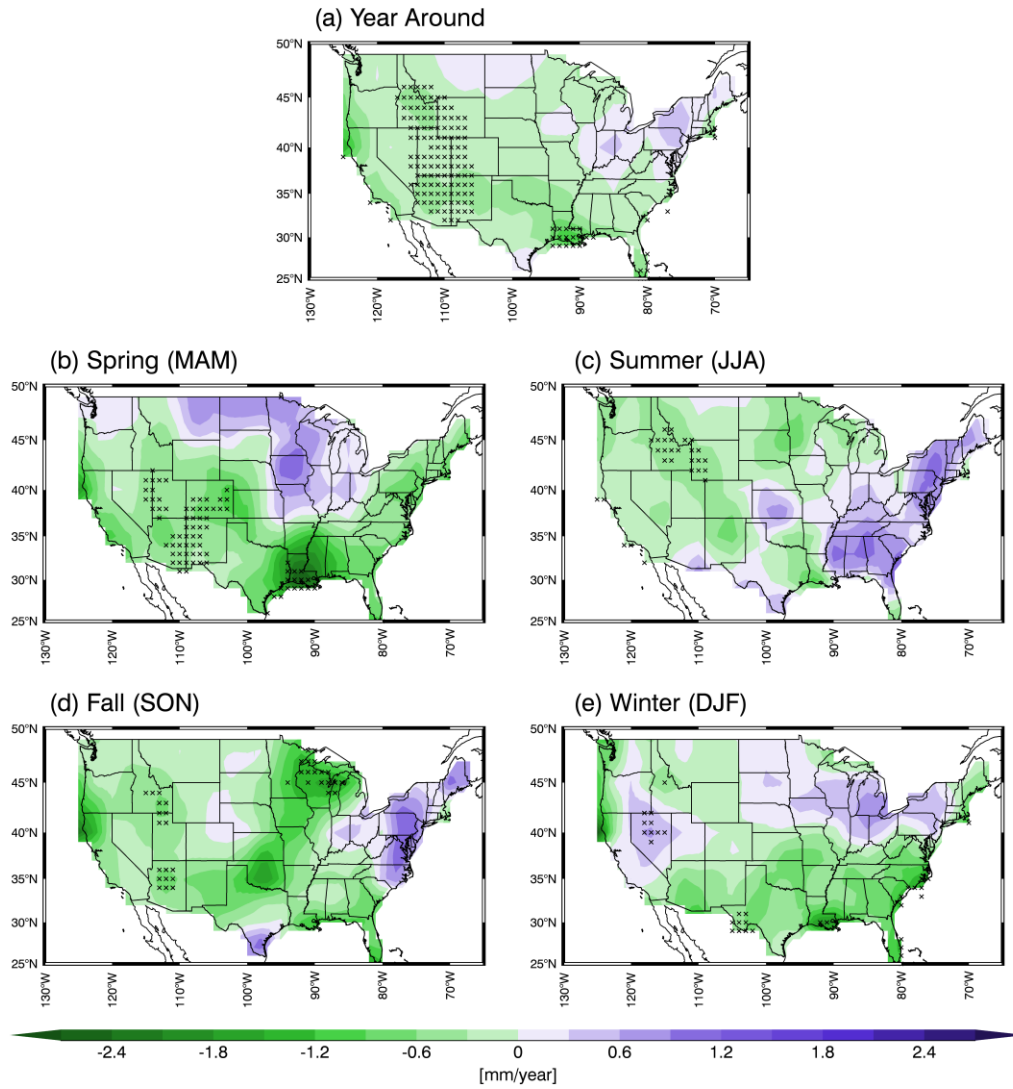
Figure 22. Spatial distribution of GPCP precipitation trend for averaged (a) annual and (b-e) seasonal precipitation during the period 1980-2013. Solid black marks indicate grid boxes that have trends are significant at the 95% confidence interval (based on the Mann-Kendall test).

precipitation amounts. Both increasing and decreasing trend rates are moderate for the annual scale, with the trends varying from -0.3 to 0.3 mm/year over most of the

CONUS. The maximum negative trends are observed over southern Louisiana, where precipitation decreases significantly by ~1.2 mm/yr. The negative trends are also evident over the mountainous regions. Compared to annual trends, the seasonal variations over different regions are significant. During spring, moderate positive trends (~0.9 mm/yr) are found over the north-central and Great Lakes regions. Whereas the decreasing trends over the south-central part of the US are more severe as high as -2.4 mm/yr. During summer asons, increasing trends are observed over eastern, central and southern boundaries of the country while decreasing trends are still found over western regions. Most of the country experiences decreasing trends during fall except for northeastern regions and southern Texas. The significant decreasing trends (~ -2.1 mm/yr) are found over southern Oregon to northern California, Oklahoma, and northern Wisconsin. Unlike the other three seasons, part of the western region shows a monotonous increasing trend, ranging from 0.0 to 0.9 mm/yr during winter. Similar to spring, positive trends are also found from the northern Great Plains to the Great Lake areas but are not as significant as during spring.

CHAPTER V

DISCUSSION

Part I: Comparison of GPCP 1DD with Q2 Estimates

The relative difference percentages (RDPs) between Q2 and GPCP 1DD estimates remain consistent in each tile from daily to yearly comparisons (Figures 2, 5 and 6) during the period 2010-2012. However, seasonal differences exist in tiles 2, 3, and 8 as the RDPs switch the sign from negative in the warm season to positive in the cold season. The different algorithms of GPCP 1DD used to estimate the precipitation between northern and southern regions may partially contribute to the RDP differences, such as between tiles 4 and 8. Correlation coefficients for monthly analyses are much higher than those for daily analyses in all tiles, which is expected due to temporal averaging. However, when transitioning from monthly to yearly analyses, the correlations in tiles 3, 4, 7, and 8 actually decrease, which is counterintuitive. This may be because the differences between Q2 and GPCP 1DD accumulated monthly estimates are in different directions or highly variable and significant decrease in sample numbers.

From Figure 3, it is noticed that during the warm season, GPCP 1DD estimates are significantly less than Q2 estimates in tile 2 (RDP=-12.83%) and tile 6 (RDP=

62

-21.26%). Since tiles 2 and 6 encompass the plains region, much of the warm season rainfall is dominated by convective precipitation, particularly in tile 6. Because of the smaller scale of the convective systems and the fact that satellite instruments are limited in spatial resolution compared to radar observations, GPCP 1DD estimates suffer from an inability to capture some daily intense precipitation events. Meanwhile, Q2 has a wet bias when estimating the accumulated precipitation from Deep Convective Systems (DCSs) during the warm season (Stenz et al. 2014; Wang et al. 2016). Therefore, the actual value of precipitation during intense convection may fall between GPCP 1DD and Q2 estimates. As a result, the accumulated warm season precipitation estimated by GPCP 1DD is less than that from Q2 for daily to yearly accumulated precipitation (Fig. 3, Tables 2, 3) for all tiles except for tile 4, where DCSs are much less frequent than in the other tiles.

The Q2 and GPCP 1DD comparisons in tile 6 are consistent with the findings in Stenz et al. (2014) and Huffman et al. (2001). Q2 daily precipitation estimates were compared with Oklahoma Mesonet observations during the period 2010-2012 with a correlation coefficient of 0.851 and a 5% wet bias during the cold season, which indicates that the Q2 precipitation estimates from NEXRAD reflectivity are reasonable for stratiform-dominated precipitation (Stenz et al. 2014). Meanwhile,

GPCP 1DD estimates display a minimum bias during winter compared to Oklahoma Mesonet observations in Huffman et al. (2001), implying that the stratiform precipitation characteristics during the cold season generally yield more accurate satellite-based estimates. Therefore, the higher correlations and smaller differences between GPCP 1DD and Q2 estimates during the cold season than the warm season in tiles 6 and 7 are anticipated due to the stratiform-dominated precipitation.

Most of the GPCP 1DD estimates are greater than Q2 estimates during the cold season, especially in the northern tiles (tiles 2-4) where the differences between GPCP 1DD and Q2 estimates are around 20%. Winter precipitation, particularly snowfall, is typically associated with shallow clouds that are close to the surface, making a radar beam more likely to overshoot falling precipitation, which may lead to underestimations in Q2 estimates. Furthermore, unlike typical warm season rainfall, which is classified into three separate groups each with its own *Z-R* relationship, there is only one *Z-R* relationship for snowfall in Q2. This relationship is designed for orographic precipitation and stratiform frozen precipitation (Zhang et al. 2011) and therefore is likely not skillful at estimating the heavier convective snowfall events. Additionally, GPCP 1DD estimates tend to overestimate precipitation amounts during the cold season, which is likely because of the difficulty satellite instruments have

when estimating frozen precipitation (McPhee and Margulis, 2005; Bolvin et al. 2009).

In tiles 3 and 4, GPCP 1DD estimates are greater than Q2 estimates for the entire year. When compared to other tiles, a more significant portion of yearly precipitation occurs during the cold season in tiles 3 and 4 than in the remaining tiles. As presented in Table 3, the Q2 and GPCP 1DD precipitation estimates during the cold season contribute approximately 35% and 46% (Q2), 41% and 47% (GPCP 1DD) to their yearly accumulated precipitation in tiles 3 and 4. Tiles 3 and 4 are located in the Great Lakes Region and the Northeastern United States, where frozen precipitation typically dominates during winter. Thus, Q2 estimates likely underestimate the precipitation over these two tiles. For the warm season, mesoscale convective systems (MCSs) in tile 4 are less frequent and generally weaker than in tiles 6 and 7. As a result, MCSs may be misclassified as stratiform events, leading to the use of inappropriate Z-R relationships and underestimation of precipitation amounts. For tile 2, although frozen precipitation is the dominant precipitation type during the cold season, a more significant portion of annual precipitation comes from warm season (79% for Q2, 73% for GPCP 1DD) than in tiles 3 and 4. Therefore, the difference between GPCP 1DD and Q2 precipitation estimates in tile 2 is much less

than those in tiles 3 and 4.

In tile 8, the difference between GPCP 1DD and Q2 estimates is relatively small throughout the year. Tile 8 is located on the East Coast of the United States, next to the Atlantic Ocean. Abundant moisture transported from the ocean and like-tropical climate lead to less variability in precipitation type. The RDPs switch the sign from positive to negative from the warm to cold season; this is likely due to the snowfall events that occur at the northern part of the tile during the cold season, which leads to underestimates in Q2.

For spatially averaged comparisons, strong correlations exist between Q2 and GPCP 1DD estimates which is expected due to large scale averaging. The two datasets also show similar spatial patterns where the precipitation estimates increase from the western Great Plains to central US (95-85ºW) as illustrated in Figures 8-9. The large precipitation estimate amount (≥1400 mm) over the central US are primarily due to the strong moisture transport from the Gulf of Mexico by the low level jet during the warm season (Dong et al. 2011). Because Q2 estimates are derived from radar retrievals and have a 1 km spatial and a 5 min temporal resolution, Q2 estimates are likely to capture more instantaneous precipitation events; particularly small scale and short period events that are not detected by the

satellite-derived GPCP 1DD estimates. Thus, Q2 estimates show more detail in precipitation variability than GPCP 1DD estimates as demonstrated in Figures 10a and 10b. Figure 10c shows the differences between Q2 and GPCP estimates and illustrates that the regions where Q2 estimates are significantly less than GPCP 1DD estimates (GPCP - Q2 > 400 mm shown in Fig. 10c) correspond well with the locations of poor radar coverage and the bottom of beam height is between ~1830 m and ~3050 m or higher, as illustrated in Fig. 1b. There are some exceptions in tile 4 where Q2 estimates are less than GPCP 1DD estimates, which is mainly due to the problems associated with *Z-R* relationships and radar overshooting problem when estimating snowfall. For the other regions where GPCP 1DD estimates are much larger than Q2 estimates, specifically from northern West Virginia down to northern Georgia, the Appalachian Mountains create beam blockage for local radars, and underestimation by Q2 likely occurs. During the cold season (Fig. 12d), the normalized differences between the two datasets over the poor radar coverage regions are much greater than those during the warm season (Fig. 11d), which is more likely because of radar over shooting problems when shallow precipitation events occurs in the regions with poor radar coverage during the cold season.

95% confidence intervals are calculated for the mean differences between GPCP

1DD and Q2 estimates for each tile. Due to a lack of physical reasoning behind GPCP

1DD or Q2 being consistently different than the other dataset in one tile, a two tailed

test was chosen using a Z value of 1.96. The confidence interval of the difference μ

is calculated by

$$\left| \frac{\bar{X}_{diff} - \mu}{\sqrt{\frac{\sigma_{diff}^{2}}{N}}} \right| \leq 1.96, \tag{2}$$

where $\bar{X}_{diff}$ is the mean difference of daily estimates between GPCP 1DD and Q2

(GPCP-Q2, mm); σ_{diff} is the standard deviation of daily estimate difference; N is

the total sample number of daily estimates for GPCP 1DD and Q2 in each tile. As

shown in Table 6, the confidence intervals are relatively small due to the large sample

Table 6. The mean differences between GPCP 1DD and Q2 daily estimates
(GPCP-Q2, mm) and their 95% confidence interval (mm) for each tile.

	Tile 2	Tile 3	Tile 4	Tile 6	Tile 7	Tile 8
All	-0.25	0.21	0.99	-0.86	-0.50	0.06
	[-0.30,	[0.12,	[0.91,	[-0.95,	[-0.59,	[-0.08,
	-0.18]	0.29]	1.06]	-0.79]	-0.41]	0.20]
Warm	-0.68	-0.28	0.84	-1.35	-0.72	-0.20
	[-0.78,	[-0.41,	[0.72,	[-1.46,	[-0.84,	[-0.40,
	-0.59]	-0.14]	0.94]	-1.23]	-0.58]	0.00]
Cold	0.33	0.73	1.15	-0.21	-0.24	0.39
	[0.28,	[0.65,	[1.05,	[-0.32,	[-0.37,	[0.20
	0.38]	0.83]	1.25]	-0.10]	-0.10]	0.58]

size of daily estimates. Most of the confidence intervals have the same sign as their mean daily difference value, indicating that most of the GPCP 1DD estimates are either larger (if both bounds of interval are greater than zero) or smaller (if both bounds of interval are less than zero) than Q2 daily estimates. With the smallest sample size among tiles and least variations of sample variances, tile 8 shows the largest range of mean differences and confidence intervals vary from negative to positive for year-around daily differences.

Compared to radar-based Q2 estimates, satellite-based GPCP 1DD estimates have coarse spatial and temporal resolutions. Furthermore, satellite instruments may have detectability issues for small scale and short duration precipitation events, especially during the warm season when intense convective precipitation events occur frequently. Therefore, Q2 estimates may provide more reasonable results than GPCP 1DD estimates over the Great Plains region during the warm season as long as the wet bias in Q2 estimates is taken into consideration. The excellent agreement between GPCP 1DD and Q2 estimates for tiles 6 and 7 during the cold season, as well as strong correlations with Oklahoma Mesonet observations for both GPCP and Q2 estimates in previous studies, indicate that GPCP and Q2 estimates can well represent the stratiform rainfall during the cold season. However, for ice phase precipitation -

especially snow over northeastern regions - GPCP 1DD estimates may be more reliable than Q2 estimates. This could be due to the issues involved with radar overshooting and *Z-R* relationship, resulting in the underestimation by Q2. Nevertheless, the accuracy of TOVS-AIRS technique used in GPCP 1DD product to estimate high latitude cold season precipitation should be determined via comparison with the high-quality surface observations. Depending on the availability of radar coverage, Q2 estimates show a discontinuity in precipitation estimates, which is also noted in Stenz et al. (2014). When using Q2, the underestimation of precipitation amounts over the regions with insufficient radar coverage should be taken into account. Fortunately, this is the kind of issue that can be avoided by satellite-based GPCP estimates.

Part II: Evaluation of Reanalyzed Precipitation Estimates and Trend Analysis

The reanalyzed precipitation estimates illustrate reasonable spatial distribution of precipitation over the CONUS when compared with GPCP SG as shown in Fig. 13, however, significant seasonal and regional differences exist (Fig. 14). Over the mountainous regions, the reanalyzed precipitation estimates are generally higher than GPCP SG precipitation throughout the year. GPCP SG may be less trustworthy over these regions because of relatively sparse GPCC gauge coverage resulting in underestimation in GPCP SG. The underestimation over orography was also found in Mcphee and Margulis (2005) and Nijssen et al. (2001) and related mainly to the relative lack of the rain gauges in mountainous regions. Meanwhile, the satellite observations, both PMW and IR, have difficulty detecting shallow, orographic precipitation (Alder et al. 2003). The precipitation amounts from GPCP show less variation than those in the reanalyses over the mountain regions (Fig. 13). Since GPCP SG has a spatial resolution of $2.5° \times 2.5°$ which is coarser than the reanalysis, it may be challenging for GPCP SG to capture small scale precipitation events which is also found in the part I of this study. Therefore, GPCP SG might not be suitable to use as a reference data for validation studies over the orography regions. However, the reliability of reanalysis precipitation estimates cannot be determined due to the

71

difficulties within models to accurately estimate precipitation over the complex terrain, and lacking of observatory upper air data to assimilate into the model. The regions where the five reanalyses significantly overestimate (RDPs > 100%) the precipitation (southern Montana extending to Utah and Colorado) correspond well with the locations where GPCP SG and the reanalysis datasets are less correlated in Fig. 15. In addition to positive biases over mountainous regions, negative biases are found in five reanalyses over the northeast part of the country especially during fall and winter when snowfall and sometimes heavier convective snowfall occur frequently, indicate that the models used in reanalysis may be less skillful in reproducing snowfall events.

ERA-Interim, MERRA2, and CFSR show very similar systematic behaviors in the spatial distribution of RDPs during different seasons (Fig. 14). These resemblances could result from assimilating similar satellite radiance data as input into their models. Underestimations are also noticed in these three reanalyses over the central part of the country, where precipitation is related to atmosphere-land interactions that may be deficiently presented in the models. During the summer time when convective precipitation events occur over the Great Plains region, more severe underestimations are found in these three reanalyses, implying that the negative biases might be caused

by the convective parameterization of the models. In the part I of this study and Huffman et al. (2001), a negative bias was found in GPCP product when estimating convective precipitation, therefore, the underestimation in reanalyses should be considered as more extreme. JRA-55 also assimilates the reprocessed radiance data from Japanese Geostationary Meteorological Satellite (GMS) and Multi-functional Transport Satellites (MTSAT), which is only used in JRA-55. Therefore, JRA-55 shows similar characteristics in RDP distribution but also shows differences over central part of the US differences (Fig. 14) compared to three reanalyses discussed above. The convective scheme adopted by JRA-55 seems to produce more realistic precipitation estimates, though it slightly overestimates the precipitation over the Plains during spring and summer.

Previous studies (Zhang et al. 2012; Rienecker et al. 2011; Robertson et al. 2011; Bosilovich et al. 2015) have shown that precipitation in reanalysis datasets is very sensitive to the observation system. For example, with the introduction of SSM/I in late 1987 and Advanced Microwave Sounding Unit-A (AMSU-A) series in late 1998, series of jumps or shifts in trend were found in MERRA and ERA-Interim global precipitation (Rienecker et al. 2011). According to Bosilovich et al. (2015), a satellite instrument on the ATOVS changed water vapor analysis at 0600 and 1800 UTC when

no radiosondes were available to anchor the analysis, and apparently lead to a decrease in range of seasonal precipitation over the central United States. In this study, however, it is noteworthy that some of the inter-annual variabilities seem to be well captured by four of five reanalyses as shown in Fig. 16 although some biases exist. Caution should be taken when use JRA-55 product because it has a consistent positive bias. Note that ERA-I shows a decreasing trend in precipitation after 1990. Simmons et al. (2010) also found this decreasing trend and concluded that it may be related to a declining shift that starts in the early 1990s due to the change in prescribed SSTs data used in ERA-I. Contradicting to JRA-55, ERA-I shows a negative bias throughout the study period. This underestimation of ERA-I is also found in Kishore et al. (2015) when compared with the gauge data over the India.

To further investigate the influence of changes in observation data, the correlation coefficients between the reanalyses and GPCP as well as their RMSEs are calculated for each month and presented in Fig. 23 and Fig. 24, respectively. ERA-I and GPCP are in good agreement throughout the entire study period except for several months that have moderate correlations (~0.75) and high RMSEs during the pre-SSM/I period. MERRA2 compares reasonably well with GPCP but performance appears to become worse after 2004. For JRA-55, a decrease in correlation coefficient is found

74
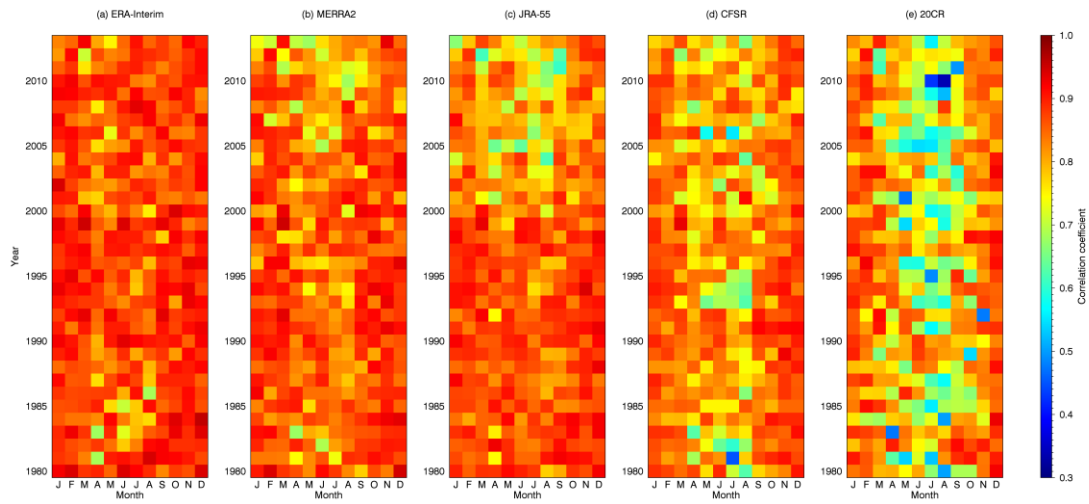
Figure 23. Correlation coefficients between reanalyses and GPCP for each monthly precipitation, x-axis represents each month, y-axis represents each year.

after mid-1999, assuming it is due to the unavailability of the atmospheric motion vectors (AMVs) data from geostationary and polar orbiting satellites (Kobayashi et al. 2015) and JRA-55 no longer uses observations from IR sensors after 2004. Zhang et al. (2012) found that CFSR has a sudden change in precipitation in 1998 resulted from the inclusion of ATOVS data. In this study, however, CFSR is relatively consistent over time. Note that during the spring and summer seasons, five reanalyses have higher RMSEs and are less correlated with GPCP which could be associated with the systematic errors of the assimilation models.
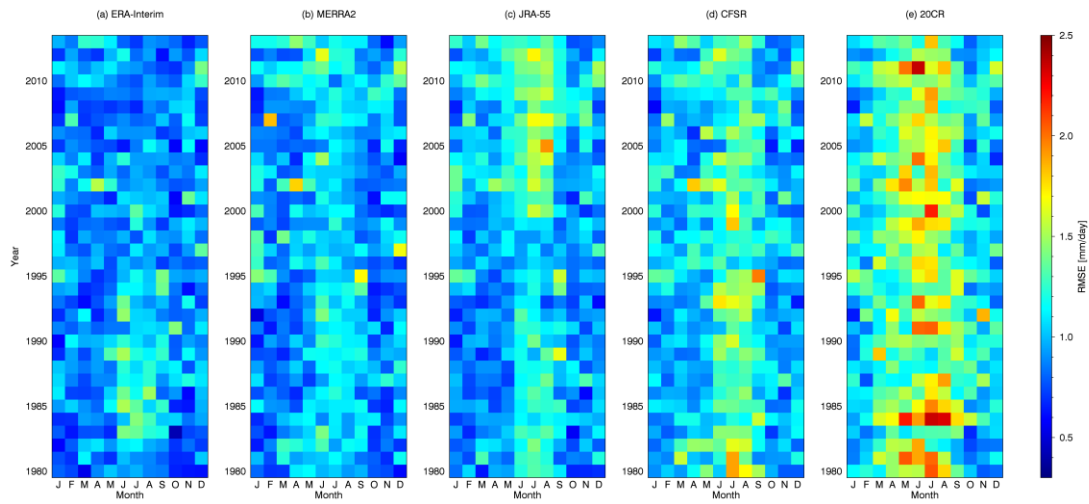
Figure 24. Similar to Fig. 23 but for RMSE.

20CR only assimilates SLP and SST observations throughout, and thus it is less sensitive to the introductions of new observing systems (Lee and Biasutti, 2014). Therefore, 20CR has less in common with other reanalyses in precipitation fields during the comparisons. Nevertheless, the biases in precipitation generated by 20CR are more significant than in the comprehensive reanalysis, regarding the highest RDPs and RMSEs throughout the year (Fig.14, Tables 4 and 5), the lowest spatial correlation coefficients (Fig. 15), and some unrealistic inter-annual variability (Fig. 16). The most possible reason is that SST and SLP data used in 20CR cannot well represent atmospheric moisture and thus the model cannot reproduce the physical and dynamical processes when generating precipitation analysis. Note that despite a dense

76

observational network and a complete sea level pressure record through the satellite era over the United States (Lee and Biasutti, 2014), the performance of the 20CR, when compared with GPCP, is still the worst among the reanalysis datasets in this study. This is not unexpected due to the simplicity of the data ingested – a sacrifice made for a longer data record.

As far as trend analysis, the results from this study are consistent with the findings from Adler et al. (2003) and Huffman et al. (2009), in that the overall precipitation amounts over the CONUS are decreasing from 1979 to present based on the GPCP data. However, from the fifth Intergovernmental panel on Climate Change (IPCC, 2014) report, an evident positive trend in annual precipitation is observed over Great Plains Region as well as the Eastern CONUS (~5 mm year^{-1} decade^{-1}) during the period 1951-2010. The decrease in precipitation is only found in small areas in the western part of the CONUS. Peterson et al. (2013) also investigated the changes in precipitation over the CONUS from 1908 to 2008 based on the gauge data. By calculating the least square trend using the second half of 100-yr period (1958-2008) minus the first half (1908-1958) period, they found negative trends in the Southwest and Southeast, while the West Coast, and great plains extending to the Northeast had positive trends, which differs from the results in this study. Nevertheless, whether the

trend present in this study is realistic and whether it is actually associated with the

changes in large-scale climate pattern or it is influenced by the changes in input data

cannot be determined because no other observation-based precipitation datasets are

available to compare with GPCP results in this study for the same study period.

CHAPTER VI

CONCLUSIONS

In the first part of study, the GPCP 1DD precipitation estimates are compared with high-quality radar estimates from NMQ Q2 over the Central and Eastern CONUS covering a total of 619 1°×1° grid boxes. The GPCP 1DD and Q2 precipitation estimates are compared over six different regions specified by the NMQ domain from January 2010 – December 2012. The temporal analyses include daily, monthly, and yearly accumulated precipitation estimates, and the spatial averages include annual, warm, and cold season estimates. In this study, we utilize the RDPs instead of NDPs to quantify the magnitude of differences between Q2 and GPCP estimates due to the relatively smaller values of NDPs which cannot well represent the differences between these two datasets. From the 3-year comparisons between Q2 and GPCP precipitation estimates, we report the following conclusions for the part I of this study:

1）Both Q2 and GPCP 1DD daily precipitation estimates show that precipitation amounts over southern tiles (6-8) are generally larger than those over northern tiles (2-4), with the most precipitation in tile 7 and the least precipitation in tile 2. Monthly accumulated precipitation and differences in

79

estimated precipitation over the six selected tiles are very similar to their daily counterparts except that correlation coefficients at the monthly scale (0.472-0.855) are much higher than those at the daily scale (0.355-0.516). However, this is not true moving from monthly to annual accumulated precipitation in tiles 4, 7, and 8 because the differences between Q2 and GPCP monthly estimates are in different directions and inadequate sample size of annual estimates over relatively short study period. RDPs between Q2 and GPCP estimates remain consistent in each tile from daily to yearly comparisons. However, there are seasonal differences of RDPs exist in tiles 2, 3, and 8 as they switch the sign from negative in the warm season to positive in the cold season.

2）During the warm season, the averages of daily precipitation from both Q2 and GPCP are generally larger than annual daily precipitation amounts, particularly in tiles 2 and 3, but correlation coefficients are slightly lower for all tiles except for tile 8. In contrast to the warm season comparisons, their counterparts during the cold season are much smaller than their annul and warm season daily precipitation estimates, especially in tile 2. Cold season correlation coefficients are slightly higher or close to their annual ones.

During the warm season, the NDPs of GPCP estimates are 10.2% less than Q2 estimates, while during the cold season, the NDPs of GPCP estimates exceed Q2 estimates by 6.6%, resulting -3.83% of the annual NDP for GPCP estimate over the CONUS.

3）For spatially averaged precipitation in each tile, excellent agreements are found between GPCP and Q2 estimates, especially for monthly accumulated precipitation with strong correlations ranging from 0.903 to 0.954. Although the difference between yearly averaged precipitation estimates is only -36.75 mm (-3.76%) over the entire study region, there are large regional differences between GPCP and Q2 estimates. Q2 estimates are much larger than GPCP estimates over central US, while in northern and northeastern regions Q2 estimates are less than GPCP estimates.

First part of this study focuses on the comparison of GPCP 1DD and Q2 estimates and gains a better understanding of advantages, weaknesses, similarities, and differences between these widely used satellite-based and radar-based precipitation estimates. In this study, for long-term estimates, GPCP 1DD and Q2 estimates both show fairly similar characteristics; however, on seasonal and regional scales large differences arise. For example, during the warm season in plain regions,

Q2 estimates might be more reliable than GPCP 1DD estimates for convective precipitation events since they accurately capture the characteristics of DCSs (Stenz et al. 2014) as long as the wet bias of Q2 estimates is accounted for. For cold season precipitation in the northern U.S., GPCP 1DD is likely a better choice for most applications because of radar overshooting issues, and the use of one *Z-R* relationship for all snowfall in Q2 estimates. Additionally, Q2 may largely underestimate the precipitation over regions with poor radar coverage, which is a problem the satellite-derived GPCP 1DD estimates can avoid. These factors should be carefully considered when using these two products for different applications.

In the part II of this study, we compare the performance of precipitation data from five recent reanalysis datasets (ERA-Interim, MERRA2, JRA-55, CFSR, and 20CR) with satellite-gauge merged GPCP SG product over the CONUS from January 1980 through December 2013. The spatial distributions and inter-annual variability of reanalyzed precipitation have been validated using GPCP SG in this study. Several statistical metrics including correlation coefficients, root-mean-square-error (RMSE), and relative difference percentage (RDP %) have been calculated to quantify the magnitude of differences between the reanalyses and GPCP SG. In addition, a trend analysis has been conducted based on the GPCP SG dataset during different seasons

(spring, summer, fall, and winter) using a sample linear regression. Based on the results from 34-yr comparisons and trend analysis, we summarize the following conclusions:

4) All of the reanalyses are able to depict reasonable spatial patterns of precipitation over the CONUS, especially for northwest part of the country. However, they generally overestimate the precipitation over the mountainous regions and underestimate over the Great Plains region throughout the year with respect to GPCP SG. Underestimations in reanalyses have also been found in northeast part of the country during fall and winter seasons. ERA-I, MERRA2, and CFSR show very similar spatial distributions of RDPs during different seasons while RDPs of 20CR are relatively different from other reanalysis datasets.

5) Compared to the annual averaged precipitation of 2.38 mm/day from GPCP SG, CFSR has the same value, ERA-Interim and MERRA2 have negative biases of 9.2% and 3.8% respectively, while JRA-55 and 20CR have positive biases of 9.7% and 12.6% respectively. For seasonal precipitation, GPCP SG ranges from 2.22 mm/day during winter to 2.61 mm/day during summer. Of all five reanalyses, CFSR has the closest seasonal means to

GPCP SG except during summer. In terms of RMSE, ERA-Interim has the lowest value varying from 0.90 to 1.05 mm/day while 20CR has the highest value with a range of 1.08 to 1.34 mm/day for annual and seasonal scales.

6) For inter-annual precipitation, 20CR and JRA-55 have positive biases while ERA-Interim has negative bias throughout the study period. Some of the inter-annual variabilities of GPCP SG precipitation are well represented by MERRA2, CFSR and JRA-55 but not by 20CR. A decreasing trend in precipitation is observed in ERA-Interim after 1990 which may be related to the prescribed SSTs data used in it.

7) For users of reanalysis product, we conclude that ERA-Interim and MERRA2 are comparatively better in representing the precipitation over the CONUS based on their performance in correlation coefficients and standard deviations against with GPCP SG estimates. Even though a decreasing trend exists in ERA-Interim, it is still the most consistent when compared against the GPCP SG.

8) For annual and seasonal accumulated precipitation derived from GPCP SG during the period from 1980 through 2013, strong annual and seasonal

cycles are found, with more than 15 years out of 34 years being outside of the 95% confidence interval range. The precipitation over the CONUS shows a negative trend throughout the study period, with an annual decreasing trend of 2.00 mm/year. Negative trends are also observed during four different seasons. For spatial trend, in addition to north central and northeastern parts of the county show positive trends, rest of the regions show negative trends for annual scale.

Overall, although reanalyses can provide realistic precipitation analysis, caution should be taken when using reanalyzed precipitation data for climate studies. For instance, errors may exist in model land-atmosphere interactions over the central United States, errors associated with model in convection and snowfall parameterizations, and the difficulties in model to accurately estimating precipitation over complex terrain. The negative bias in ERA-Interim as well as the positive bias in JRA-55 should be also taken into account for their users. Even though the changes in observing system seem to have less influence on the continuity of precipitation over the CONUS, they might still cause inhomogeneities in reanalyzed climate over other parts of the world where radiosonde data is less dense compared to the United States and their estimated precipitation is highly dependent upon satellite

observations, such as over oceans and Africa. Furthermore, the general type and quality of assimilated data will affect the performance of reanalyses. The comprehensive reanalyses (ERA-Interim, CFSR, JRA-55, MERRA2) that assimilate both satellite retrievals and upper air information show comparatively better performance in presenting precipitation than simple reanalysis (20CR) that only assimilates SST and SLP data. We do understand there are errors and uncertainties affiliated with GPCP product, and they are considered when comparing with reanalysis datasets and are discussed in this paper. The results presented in this study provide useful information to the limitations and strengths of each reanalysis datasets, lead to better utilization by their users, and suggesting substantial efforts are necessary to further improve the reanalysis precipitation estimates in the future.

Appendix

List of Abbreviations

Table 6. List of Abbreviations

Abbreviation	Full Text
AIRS	Advanced Infrared Sounder
AMSU-A	Advanced Microwave Sounding Unit-A
APHRODITE	Asian Precipitation-Highly-Resolved Observational Data Integration Towards Evaluation of the Water Resources
ATOVS	Advanced TIROS Operational Vertical Sounder
CAMS	Climate Analysis and Monitoring System
CFSR	Climate Forecast System Reanalysis
CIRES	Cooperative Institute for Research in Environmental Sciences
CMAP	Climate Prediction Center merged Analysis of Precipitation
CMORPH	Climate Prediction Center morphing technique
CONUS	Continental United States
CPC	Climate Prediction Center
DAS	Data assimilation system
DCAPE	Downward Convective Available Potential Energy
DMSP	Defense Meteorological Satellite Program
ECMWF	European Centre for Medium-Range Weather Forecasts
GEOS-5	Goddard Earth Observing System Model version 5
GEWEX	Global Energy and Water Exchanges Project
GFS	Global Forecast System
GHCN	Global Historical Climate Network
GMS	Geostationary Meteorological Satellite
GOES	Geostationary Operational Environmental Satellite
GPCC	Global Precipitation Climatology Centre
GPCP	Global Precipitation Climatology Project
GPM	Global Precipitation Mission
GPROF	Goddard Profiling Algorithm
GSPDC	Geostationary Satellite Precipitation Data Centre
IMERG	Integrated Multi-Satellite Retrievals
IPCC	Intergovernmental panel on Climate Change
IR	Infrared

JMA	Japanese Meteorological Agency
JRA-25	Japanese 25-year Reanalysis
JRA-55	Japanese 55-year Reanalysis
MERRA	Modern-Era Retrospective analysis for Research and Applications
MERRA2	MERRA2 version2
MOM4	Modular Ocean Model version 4
MTSAT	Multi-functional Transport Satellites
NASA	National Aeronautics and Space Administration
NCAR	National Center for Atmospheric Research
NCEP	National Centers of Environmental Prediction
NDP	Normalized Difference Percentage
NEXRAD	Next-Generation Radar
NMQ Q2	National Mosaic and Multi-Sensor Next Generation Quantitative Precipitation Estimation System
NOAA	National Oceanic and Atmospheric Administration
OLR	Outgoing longwave radiative
OPI	OLR Precipitation Index
PACRAIN	Pacific Rainfall Database
PERSIANN	Precipitation Estimation from Remotely Sensed Information Using Artificial Neural Networks
PMW	Passive microwave
RDP	Relative Difference Percentage
RMSE	Root-Mean Squared Error
SG	Satellite-gauge
SLP	Sea level pressure
SSIMS	Special Sensor Microwave Imager-Sounder
SST	Sea surface temperature
TIROS	Television Infrared Operational Satellite
TMI	TRMM Microwave Imager
TRMM	Tropical Rainfall Measuring Mission
TMPA	Tropical Rainfall Measuring Mission Multi-Satellite Precipitation Analysis
TMPI	Threshold-Matched Precipitation Index
TOVS	TIROS Operational Vertical Sounder
WSR-88D	Weather Surveillance Radar-1988 Doppler
1DD	One Degree Daily

20CR	20th Century Reanalysis

REFERENCES

Adler, R. F., and Coauthors, 2003: The Version-2 Global Precipitation Climatology Project (GPCP) Monthly Precipitation Analysis (1979-present). *J. Hydrometeor.*, **4**, 1147-1167.

Alemohammad, S. H., K. A. McColl, A.G. Konings, D. Entekhabi, and A. Stoffelen, 2015: Characterization of precipitation product errors across the United States using multiplicative triple collocation. *Hydrol. Earth Syst. Sci.*, **19**, 3489–3503.

Arakawa, A., and W. H. Schubert, 1974: Interaction of a cumulus cloud ensemble with the large-scale environment, Part I. *J. Atmos. Sci*., **31**, 674–701.

Arkin, P. A., and B. N. Meisner, 1987: The relationship between large-scale convective rainfall and cold cloud over the Western Hemisphere during 1982–1984. *Mon. Wea. Rev*., **115**, 51–74.

Ashouri, H., K. L. Hsu, S. Sorooshian, D. K. Braithwaite, K. R. Knapp, D. L. Cecil, B. R. Nelson, and P. O. Prat, 2015: PERSIANN-CDR: Daily precipitation climate data record from multisatellite observations for hydrological and climate studies, *Bull. Am. Meteorol. Soc*., **96**, 69–83.

Benton, G. S. and M. A. Estoque, 1954: Water-vapor transfer over the North American continent. *J. Meteor*, **11**, 462-477.

Bosilovich, M. G., 2013: Regional climate and variability of NASA MERRA and recent reanalyses: U.S. summertime precipitation and temperature. *J. Appl. Meteor. Climatol*., **52**, 1939–1951, doi:10.1175/JAMC-D-12-0291.1.

Bosilovich, M. G., J. Chen, F. R. Robertson, and R. F. Adler, 2008: Evaluation of global precipitation in reanalyses. *J. Appl. Meteor. Climatol*., **47**, 2279–2299.

Bosilovich, M., R. Lucchesi, and M. Suarez (2015), MERRA-2: File Specification. GMAO Office Note 9 (Version1.0)*, 73 pp. [Available from* http://gmao/gsfc/nasa/gov/pubs/office_notes.*]*

Bolvin, D. T., R. F. Adler, G. J. Huffman, E. J. Nelkin, J. P. Poutiainen, 2009: Comparison of GPCP monthly and daily precipitation estimates with high-latitude gauge observations. *J. Appl. Meteor.*, **48**, 1843-1857.

Blacutt, L. A., D. L. Herdies, L. G. G. De Gonçalves, D. A. Vila, and M. Andrade, 2015: Precipitation comparison for the CFSR, MERRA, TRMM3B42 and Combined Scheme datasets in Bolivia. *Atmos. Res*, **163**, 117-131.

Burnett, A. W., M. E. Kirby, H. T. Mullins, and W. P. Patterson, 2003: Increasing Great Lake-effect snowfall during the twentieth century: A regional response to global warming? *J. Climate*, **16**, 3535–3541.

Chen, S., and Coauthors, 2013: Evaluation and uncertainty estimation of NOAA/NSSL Next-Generation National Mosaic Quantitative Precipitation Estimation Product (Q2) over the continental United States. *J. Hydrometeor.*, **14**, 1308–1322.

Compo, G. P., and Coauthors, 2011: The Twentieth Century Reanalysis Project. *Quart. J. Roy. Meteor. Soc.*, **137**, 1–28.

Cui, W., X. Dong, B. Xi, and R. Stenz, 2016: Comparison of the GPCP 1DD precipitation product and NEXRAD Q2 precipitation estimates over the Continental United States. *J. Hydrometeor.* **17**, 1837-1853.

Davis, R. E., R. Dolan, and G. Demme, 1993: Synoptic climatology of Atlantic coast northeasters. *Int. J. Climatol.*, **13**, 171–189

Dee, D., and Coauthors, 2011: The ERA-Interim reanalysis: Configuration and performance of the data assimilation system. *Quart. J. Roy. Meteor. Soc.*, **137**, 553–597.

Dolinar, E. K., X. Dong and B. Xi, 2015: Evaluation and intercomparison of clouds, precipitation, and radiation budgets in recent reanalyses using satellite-surface observations. *Climate. Dynam.*, 1-22.

Dong, X., B. Xi, A. Kennedy, Z. Feng, J. Entin, P. Houser, B. Schiffer, W. Olson, T. L'Ecuyer, T. Liu, K-L Hsu, B. Lin, Y. Deng, and T. Jiang, 2011: Investigation the 2006 Drought and 2007 Flood Extreme Events at the SGP through an Integrative Analysis of Observations. *J. Geophys. Res*. 116, D03204, doi:10.1029/2010JD014776.

Fensholt R., and K. Rasmussen, 2011: Analysis of trends in the Sahelian 'rain-use efficiency' using GIMMS NDVI, RFE and GPCP rainfall data. *Remote Sens. Environ*., **115**, 438–451.

Fulton, R., J. Breidenbach, D. J. Seo, D. Miller, and T. O'Bannon, 1998: The WSR-88D rainfall algorithm. *Wea. Forecasting.*, **13**, 377–395.

Gebremichael, M., W. F. Krajewski, M. L. Morrissery, G. J. Huffman, R. F. Adler, 2005: A detail evaluation of GPCP 1° daily rainfall estimates over the Mississippi river basin. *J. Appl. Meteor.*, **44**, 665-681.

Grams, H., 2013: NMQ update summer 2013: Important user information. Accessed 2 May 2016. [Available online at docs.google.com/document/d/1Op3uETOtd28YqZffgvEGoIj0qU6VU966iT_QNUOmqn4/edit.]

Grody, N. C., 1991: Classification of snow cover and precipitation using the Special Sensor Microwave/Imager (SSM/I). *J. Geophys. Res.,* **96**, 7423–7435.

Gruber, A., and V. Levizzani, 2008: Assessment of global precipitation products: A project of the World Climate Research Programme Global Energy and Water Cycle Experiment (GEWEX) Radiation Panel. WCRP-128, WMO/TD-1430, 57 pp.

Gu, G., R. F. Adler, G. J. Huffman, and S. Curtis, 2007: Tropical rainfall variability on interannual-to-interdecadal/longer-time scales derived from the GPCP monthly product. *J. Clim.,* **20**, 4033–4046.

Hatzianastassiou, N., C. D. Papadimas, C. J. Lolis, A. Bartzokas, V. Levizzani, J. D. Pnevmatikos, and B. D. Katsoulis, 2016: Spatial and temporal variability of precipitation over the Mediterranean Basin based on 32-year satellite Global Precipitation Climatology Project data, part I: evaluation and climatological patterns. *Int. J. Climatol.*

Holzman, B., 1937: Sources of moisture for precipitation in the United States. US Department of Agriculture.

Huffman, G. J., R. F. Adler, M. Morrissey, D. T. Bolvin, S. Curtis, R. Joyce, B. McGavock, and J. Susskind, 2001: Global precipitation at one-degree daily resolution from multisatellite observations. *J. Hydrometeor.*, **2**, 36–50.

—, —, D. T. Bolvin, and G. Gu, 2009: Improving the global precipitation record: GPCP version 2.1. Geophys. *Res. Lett*., **36**, L17808, doi:10.1029/2009GL040000.

—, —, M. M. Morrissey, D. T. Bolvin, and G. Gu, 2009: Improving the global precipitation record: GPCP Version 2.1. *Geophys. Res. Lett.*, **31**, L06116.

—, —, D. T. Bolvin, and E. Nelkin, 2010: The TRMM Multi-Satellite Precipitation Analysis. Satellite Rainfall Applications for Surface Hydrology, F. Hossian and M. Gebremichael, Eds., Springer, 3–22.

—, and D. T. Bolvin, 2012: GPCP version 2.2 combined precipitation data set. NCDC, Asheville, NC, 46 pp. [*Available online at ftp://precip.gsfc.nasa.gov/pub/gpcp-v2.2/doc/V2.2_doc.pdf.*]

—, —, 2013: Version 1.2 GPCP one-degree daily precipitation data set documentation. GPCP. *[Available online at ftp://rsd. gsfc. nasa. gov/pub/1dd-v1. 2/1DD_v1. 2_doc. pdf.]*

—, —, D. Braithwaite, K. Hsu, R. Joyce, and P. Xie, 2014: NASA Global Precipitation Measurement (GPM) Integrated Multi-Satellite Retrievals for GPM (IMERG). NASA GSFC Algorithm Theoretical Basis Doc., version 4.4, 30 pp.

—, and Coauthors, 2007: The TRMM Multisatellite Precipitation Analysis (TMPA): Quasi-global, multiyear, combined-sensor precipitation estimates at fine scales. *J. Hydrometeor.*, **8**, 38–55, doi:10.1175/JHM560.1.

Joyce, R. J., J. E. Janowiak, P. A. Arkin, and P. Xie, 2004: CMORPH: A method that produces global precipitation estimates from passive microwave and infrared data at high spatial and temporal resolution. *J. Hydrometeor.*, **5**, 487–503.

Joshi, M. K., Rai, A. and Pandey, A. C. (2013), Validation of TMPA and GPCP 1DD against the ground truth rain-gauge data for Indian region. *Int. J. Climatol.*, **33**, 2633–2648.

Kalnay, E., 1996: The NCEP/NCAR 40-year Reanalysis Project. *Bull Amer Meteo Soc,* 77, **3**, 437–471.

Kanamitsu, M., W. Ebisuzaki, J. Woollen, S-K. Yang, J. J. Hnilo, M. Fiorino, and G. L. Potter, 2002: NCEP-DOE AMIP-II Reanalysis (R-2). *Bull. Amer. Meteor. Soc.*, **83**, 1631–1643.

Kishore, P., S. Jyoth, G. Basha, S. V. B. Rao, M. Rajeevan, I. Velicogna , T. C. Sutterley, 2016: Precipitation climatology over India: validation with observations and reanalysis datasets and spatial trends. *Clim Dyn.* doi:10. 1007/s00382-015-2597-y

Kobayashi, S., and Coauthors, 2015: The JRA-55 Reanalysis: General specifications and basic characteristics. *J. Meteor. Soc.* Japan, **93**, 5–48, doi:10.2151/jmsj.2015-001.

Kummerow, C., W. S. Olson and L. Giglio, 1996: A simplified scheme for obtaining precipitation and vertical hydrometeor profiles from passive microwave sensors. IEEE Trans. Geosc. Rem. Sen., **24**, 1213 -1232.

Lee, D. E., and M. Biasutti, 2014: Climatology and variability of precipitation in the Twentieth Century Reanalysis. *J. Climate*, **27**, 5964–5981, doi:10.1175/JCLI-D-13-00630.1.

Ma, L., T. Zhang, O. W. Frauenfeld, B. Ye, D. Yang, and D. Qin, 2009: Evaluation of precipitation from the ERA-40, NCEP-1, and NCEP-2 reanalyses and CMAP-1, CMAP-2, and GPCP-2 with ground-based measurements in China. *J. Geophys. Res*., **114**, D09105. doi:10.1029/2008JD011178.

Marshall, J. S., W. Hitschfeld, and K. L. S. Gunn, 1955: Advances in radar weather. Advances in Geophysics, Vol. 2, Academic Press, 1–56.

Mcphee, J., and S. A. Margulis, 2005: Validation and error characterization of GPCP-1DD precipitation product over the Contiguous United States. *J. Hydrometeor.*, **6**, 441-459.

Molod A M, Takacs L L, Suarez M and Bacmeister J 2015 Development of the GEOS-5 atmospheric general circulation model: evolution from MERRA to MERRA2. *Geosci. Model. Dev.,* **8**, 1339–56.

Moorthi, S., and M. J. Suarez, 1992: Relaxed Arakawa-Schubert. A parameterization of moist convection for general circulation models. *Mon. Wea. Rev*., **120**, 978–1002.

Nakagawa, M., and A. Shimpo, 2004: Development of a cumulus parameterization scheme for the operational global model at JMA. RSMC Tokyo-Typhoon Center Tech. Review 7, Japan Meteorological Agency, 10–15.

Onogi, K., and Coauthors, 2007: The JRA-25 reanalysis. *J. Meteor. Soc. Japan*, **85**, 369–432.

Pachauri, R. K., and Coauthors, 2014: Climate change 2014: synthesis Report. Contribution of working groups I, II and III to the fifth assessment report of the intergovernmental panel on climate change. IPCC.

Prakash, S., R. M. Gairola, and A. K. Mitra, 2015: Comparison of large-scale global land precipitation from multisatellite and reanalysis products with gauge-based GPCC data sets. *Theor. Appl. Climatol.*, 121.1-2: 303-317.

Pfeifroth, U., R. Mueller, and B. Ahrens, 2013: Evaluation of satellite-based and reanalysis precipitation data in the tropical Pacific. *J. Appl. Meteor. Climatol*., **52**, 634–644, doi:10.1175/JAMC-D-12-049.1.

Randall, D. A., and D. M. Pan, 1993: Implementation of the Arakawa– Schubert cumulus parameterization with a prognostic closure. *Bull. Amer. Meteor. Soc*, **74**, 137–144.

Rana, S., J. McGregor, and J. Renwick, 2015: Precipitation Seasonality over the Indian Subcontinent: An Evaluation of Gauge, Reanalyses, and Satellite Retrievals. *J. Hydrometeor*, **16**, 631–651.

Rienecker, M. M., and Coauthors, 2008: The GEOS-5 Data Assimilation System—Documentation of versions 5.0.1, 5.1.0, and 5.2.0. NASA Tech. Rep. NASA/TM-2008-104606, Vol. 27, 92 pp.

Rienecker, M. M., and Coauthors, 2011: MERRA: NASA's Modern-Era Retrospective Analysis for Research and Applications. *J. Climate*, **24**, 3624– 3648.

Robertson, F. R., M. G. Bosilovich, J. Chen, and T. L. Miller, 2011: The effect of satellite observing system changes on MERRA water and energy fluxes. *J. Climate*, **24**, 5197–5217.

Rosenfeld, D., D. B. Wolff, and D. Atlas, 1993: General probability-matched relations between radar reflectivity and rain rate. *J. Appl. Meteor.*, **32**, 50–72.

Saha, S., and Coauthors, 2010: The NCEP Climate Forecast System Reanalysis. *Bull. Amer. Meteor. Soc*., **91**, 1015–1057.

Simmons, A., K. M. Willett, P. D. Jones, P. W. Thorne, and D. P. Dee, 2010: Low-frequency variations in surface atmospheric humidity, temperature, and precipitation: Inferences from reanalyses and monthly gridded observational data sets. *J. Geophys. Res*., **115**, D01110, doi:10.1029/2009JD012442.

Sorooshian, S., K.L. Hsu, X. Gao, H. V. Gupta, B. Imam, and D. Braithwaite, 2000: Evaluation of PERSIANN system satellite-based estimates of tropical rainfall. *Bull. Amer. Meteor. Soc*., **81**, 2035–2046.

Stanfield R, Dong X, Xi B, Del Genio A, Minnis P, Doelling D, Loeb N (2015) Assessment of NASA GISS CMIP5 and post-CMIP5 simulated clouds and TOA radiation budgets using satellite observations. Part II: TOA radiation budgets and cloud radiative forcings. *J Climate,* **28**:1842–1864. doi:10.1175/ JCLI-D-14-00249.1.

Stenz, R., X. Dong, B. Xi, R. J. Kuligowski, 2014: Assessment of SCaMPR and NEXRAD Q2 precipitation estimates using Oklahoma Mesonet observations. *J. Hydrometeor.*, **15**, 2484 - 2500.

Sundqvist, H., 1978: A parameterization scheme for non-convective condensation including prediction of cloud water content. *Quart. J. Roy. Meteor. Soc*., **104**, 677–690.

Susskind, J., and J. Pfaendtner, 1989: Impact of interactive physical retrievals on NWP. Report on the Joint ECMWF/EUMETSAT Workshop on the Use of Satellite Data in Operational Weather Prediction: 1989–1993, *T. Hollingsworth, Ed.*, Vol. 1, ECMWF, 245–270.

Susskind, J., P. Piraino, L. Rokke, T. Iredell, and A. Mehta, 1997: Characteristics of the TOVS Pathfinder Path A dataset. *Bull. Amer. Meteor. Soc.*, **78**, 1449–1472.

Tian, Y., C. D. Peters-Lidard, 2010: A global map of uncertainties in satellite-based precipitation measurements. *J. Geophys. Res*., 37: L24407.

Villarini, G., P. V. Mandapaka, W. F. Krajewski, R. J. Moore, 2008: Rainfall and sampling uncertainties: A rain gauge perpective. *J. Geophys. Res*., 113 (2008).

Wang, J., X. Dong, B. Xi, and A. J. Heymsfield, 2015: Investigation of liquid cloud microphysical properties of DCS: Parameterization and precipitation retrieval of stratiform rain. Accepted by *J. Geophys. Res.*

Wang, A., and X. Zeng, 2012: Evaluation of multireanalysis products with in situ observations over the Tibetan Plateau. *J. Geophys. Res*., **117**, D05102, doi:10.1029/2011JD016553.

Wilheit, T., A. Chang, and L. Chiu, 1991: Retrieval of monthly rainfall indices from microwave radiometric measurements using probability distribution functions. *J. Atmos. Oceanic Technol*., **8**, 118–136.

Wilson, J., and E. A. Brandes, 1979: Radar measurement of rainfall–A summary. *Bull. Amer. Meteor. Soc.*, **60**, 1048–1058.

Whitaker, J. S., and T. M. Hamill, 2002: Ensemble data assimilation without perturbed observations. *Mon. Wea. Rev*., **130**, 1913–1924.

Wu, W., D. Kitzmiller, and S. Wu, 2012: Evaluation of radar precipitation estimates from the National Mosaic and Multisensor Quantitative Precipitation Estimation System and the WSR- 88D precipitation processing system over the conterminous United States. *J. Hydrometeor.*, **13**, 1080–1093.

Xie, P., and P. A. Arkin, 1997: Global Precipitation: A 17-Year Monthly Analysis Based on Gauge Observations, Satellite Estimates, and Numerical Model Outputs. *Bull. Amer. Meteor. Soc.*, **78**, 2539–2558.

Xie, P., and P. A. Arkin, 1998: Global monthly precipitation estimates from satellite-observed outgoing longwave radiation. *J. Climate*, **11**, 137–164.

Xie, P., J. E. Janowiak, P. A. Arkin, R. F. Adler, A. Gruber, R. Ferraro, G. J. Huffman, and S. Curtis, 2003: GPCP pentad precipitation analyses: An experimental dataset based on gauge observations and satellite estimates. *J. Climate*, **16**, 2197–2214.

Zhang, J., and Coauthors, 2011: National Mosaic and MultiSensor QPE System: Description, results, and future plans. *Bull. Amer. Meteor. Soc.*, **92**, 1321–1338.

Zhao, Q. Y., and F. H. Carr, 1997: A prognostic cloud scheme for operational NWP models. *Mon. Wea. Rev*., **125**, 1931–1953.

Zhang, L., A. Kumar, and W. Wang, 2012: Influence of changes in observations on precipitation: A case study for the Climate Forecast System Reanalysis (CFSR). *J. Geophys. Res*., **117**, D08105, doi:10.1029/2011JD017347.